Electronic Supporting Information

Porous zeolitic imidazolate frameworks assembled with highly-flattened tetrahedral copper(II) centres and 2-nitroimidazolates

Cheolwon Jung, [a] Sang Beom Choi, [b] Jaewoo Park, [c] Minji Jung, [c] Jonghoon Kim, [b] Hyunchul Oh*[c,d] and Jaheon Kim*[a]

[a] Department of Chemistry,Soongsil University, Seoul 06978, Republic of Korea.
[b] Integrative Institute of Basic Science, Soongsil University, Seoul 06978, Republic of Korea
[c] Department of Chemistry, Ulsan National Institute of Science and Technology, Ulsan 44919, Republic of Korea
[d] Graduate School of Carbon Neutrality
[e] Ulsan National Institute of Science and Technology, Ulsan 44919, Republic of Korea

Contents

Section 1. General Methods

Copper(II) nitrate trihydrate ($Cu(NO_3)_2 \cdot 3H_2O$), copper(I) chloride (CuCl), and imidazole (ImH) were purchased from Sigma-Aldrich. Imidazole-2-carboxaldehyde and 2-nitroimidazole were purchased from Tokyo Chemical Industry. N,N-dimethylformamide (DMF), 1-methyl-2-pyrrolidone (N-methylpyrrolidone, NMP), methanol, diethyl ether, nitric acid (60% solution in water), and sulfuric acid were purchased from Daejung Chemicals & Metals Co., Ltd. All chemicals were used without further purification.

Elemental analysis was performed with a Thermo Scientific Flash 2000 HT analyzer. Powder X-ray diffraction (PXRD) data were collected on a Rigaku MiniFlex diffractometer with CuKα radiation (λ = 1.5418 Å). Single crystal X-ray diffraction (SCXRD) data were collected with synchrotron radiation on a Rayonix MX225HS CCD area detector at the BL2D-SMC beamline at Pohang Accelerator Laboratory (PAL). Thermogravimetric analyses (TGA) were carried out using a PerkinElmer Pyris 1 in the air at a heating rate of 5 °C/min. Fourier transform infrared (FT-IR) spectra were measured employing a PerkinElmer FT/IR using the samples prepared as KBr pellets. ^{1}H-NMR spectra were recorded with a Bruker 400 MHz NMR spectrometer. Field emission-scanning electron microscope (FE-SEM) images were obtained using the Carl Zeiss GeminiSEM 300 at 10 kV.

The conventional low-pressure N_2 adsorption-desorption isotherms were measured using the standard volumetric procedure on a BELSORP-mini (BEL-Japan, INC.) equipment. Typically, ~100 mg of a dried Cu-ZIF sample on a Schlenk line was loaded in a sample tube, and heated at 160 °C for 12 hours in vacuum (< 1.0×10^{-3} Torr) before gas adsorption experiments. The dead volume of the sample tube was automatically measured with He gas. All used gases were ultrahigh purity grade (99.9999 %). Before measuring, each sample was dried and fully degassed at 160 ºC for 10 h (Cu-ZIF-**gis**) or 120 ºC for 6 h (Cu-ZIF-**rho**) under vacuum (< 1.0×10^{-3} Torr). The dead volume of the sample cell was automatically measured using helium gas. Pressure equilibrium points were also collected automatically by the equipment for adjusted equilibrium time. The weight of each sample was measured after the measurement. The measurement temperature was maintained using a liquid nitrogen or argon bath or an ethylene glycol/water circulator.

The high-pressure gas (H_2, CO_2, and CH_4) sorption isotherms were measured using the standard volumetric procedure on a BELSORP-HP instrument (BEL-Japan, INC.). Typically, 0.5~1.0 g of a dried Cu-ZIF sample on a Schlenk line was loaded in a sample tube, and heated at 160 °C for 12 hours in vacuum (< 1.0×10^{-3} Torr) before gas adsorption experiments. The dead volume of the sample tube was automatically measured with He gas. All used gases were ultrahigh purity grade (99.9999 %).

Section 2. Syntheses and Characterizations

2.1. Cu-ZIF-**gis**

Crystals. $Cu(NO_3)_2 \cdot 3H_2O$ (24.2 mg, 0.10 mmol) and 2-nitroimidazole (nImH) (22.6 mg, 0.20 mmol) were dissolved in DMF (3.0 mL) in a 8 mL vial. The vial was tightly capped, and heated in a temperature-fixed oven at 80 °C for 24 hours. The produced blue square crystals were filtered and washed with neat DMF (3 mL × 3) and diethyl ether (3 mL × 3), and dried under reduced pressure for 1 day. The yield was 44.5% based on 1 mole of $Cu(NO_3)_2 \cdot 3H_2O$. Elemental microanalysis for $Cu(nIm)_2$ = $C_6H_4N_6O_4Cu$: Calcd.: C, 25.05; H, 1.40; N, 29.22 %. Found: C, 25.07; H, 1.37; N, 29.39 %.

The reaction proceeds without any problems up to a 10× scale. However, at a 30× scale, brown crystals (Cu(nIm)) are also produced (Fig. S6). A hydrothermal reaction ($Cu(NO_3)_2 \cdot 3H_2O$, 24.2 mg; 2-nitroimidazole, 22.6 mg; water, 10 mL; T = 80 °C; t = 24 h) also can give Cu-ZIF-**gis** but the brown crystals are also produced as a minor product.

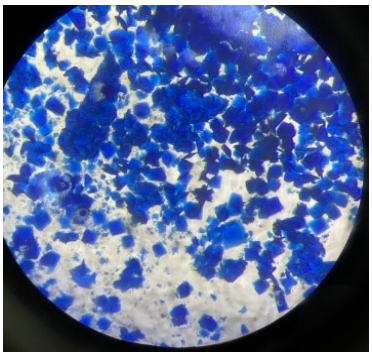

Fig. S1. An optical microscope image of Cu-ZIF-**gis** crystals.

When the reaction mixture for Cu-ZIF-**gis** was heated for more than a day, brown needle crystals appeared (Fig. S6); the synthesis of the brown crystals is discussed in the latter part of this section.

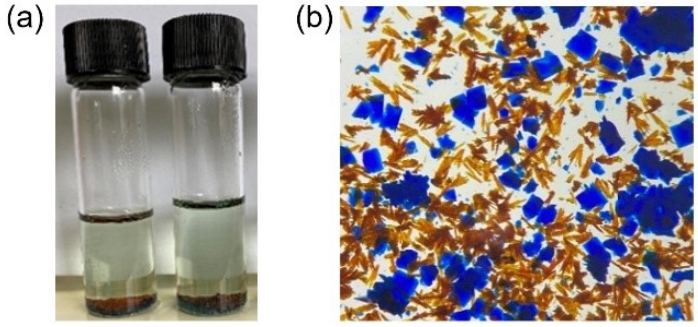

Fig. S2. (a) The reaction mixture for Cu-ZIF-**gis** heated for 2 days. (b) An optical microscope image of the product mixture was taken from the vials in (a).

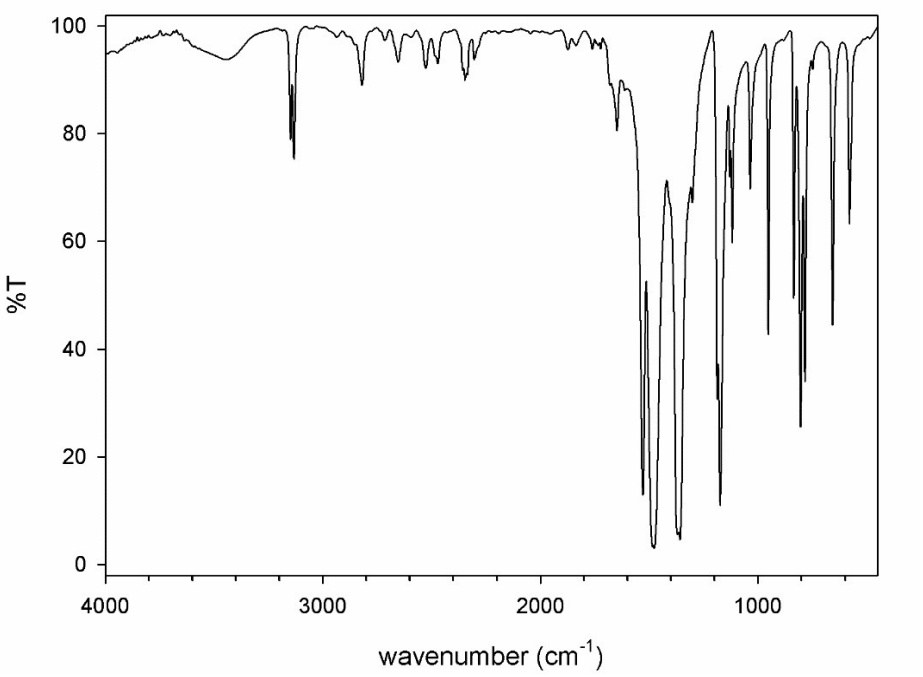

Fig. S3. The IR spectrum of the microcrystalline Cu-ZIF-**gis.**

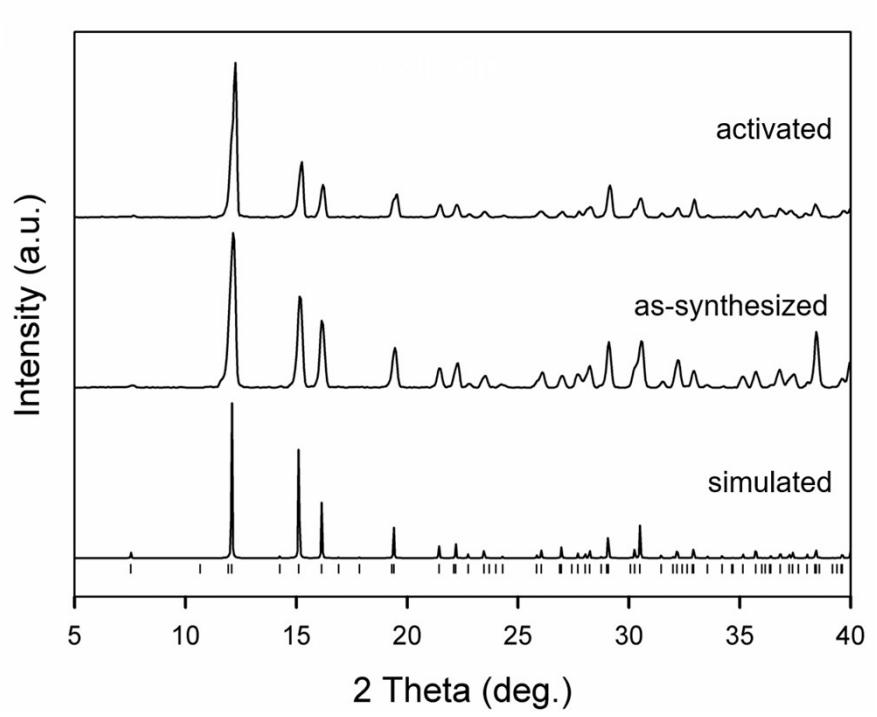

Fig. S4. The measured and simulated PXRD patterns for Cu-ZIF-**gis**. The activated sample was obtained by heating Cu-ZIF-**gis** at 160 °C for 10 h.

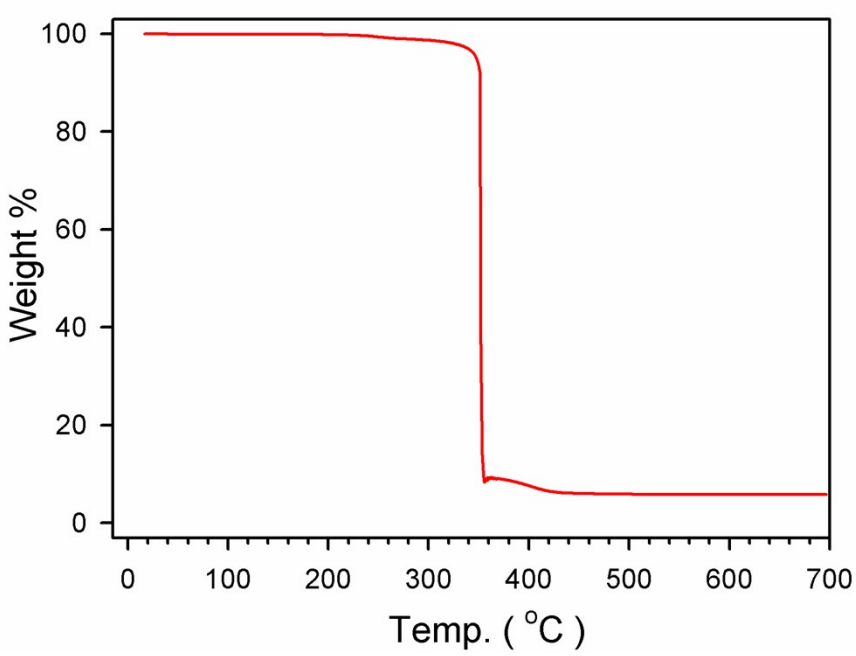

Fig. S5. The TGA thermogram of Cu-ZIF-**gis** heated at 5 °C/min in air.

We adjusted the reaction conditions to obtain phase-pure brown crystals. 2-Nitroimidazole (0.20 mmol) and $Cu(NO_3)_2 \cdot 3H_2O$ (0.10 mmol) were placed in an 8 mL vial and dissolved in DMF solvent (3.0 mL). After adding 0.2 mL of 5M H_2SO_4 solution, the capped vial was heated in a temperature-fixed oven at 90 °C for 48 hours. The collected solid was washed with neat MeOH (3 mL × 3) and diethyl ether (3 mL × 3), and dried under reduced pressure for 1 day. Elemental microanalysis for Cu(nIm) = $C_3H_2N_3O_2Cu$: Calcd.: C, 25.05; H, 1.15; N, 23.93 %. Found: C, 25.60; H, 1.11; N, 24.13 %.

As the crystal diffracted X-ray very weakly, the crystal structure could not be elucidated.

In the ^{1}H-NMR spectrum of the brown crystals, only a 2-nitroimidazole signal was observed (Fig. S10).

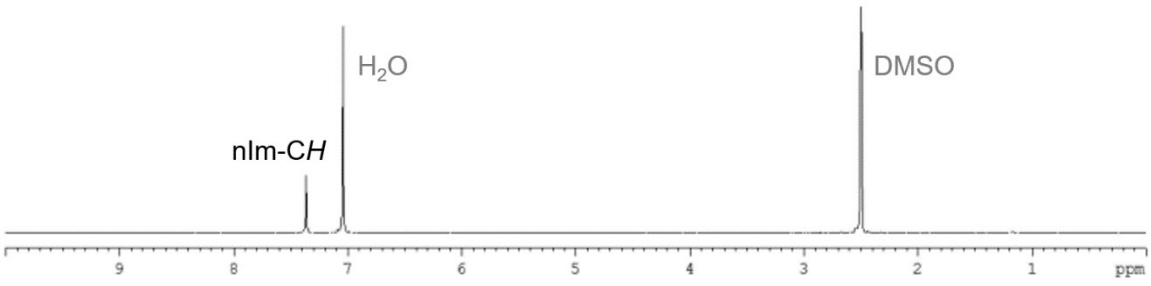

Fig. S6. The ^{1}H-NMR spectrum of Cu(nIm) brown crystals dissolved in DCl (20 μL)/DMSO-d_6 (0.5 mL).

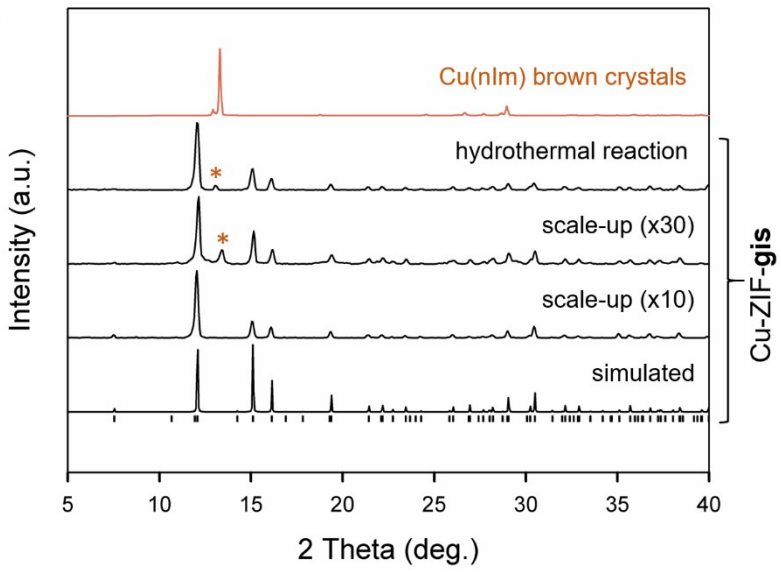

Fig. S7. The measured PXRD pattern of the Cu(nIm) brown crystals is compared with those of the Cu-ZIF-**gis** products obtained under different reaction conditions.

2.2. Cu-ZIF-**rho**

Crystals (Method A). $Cu(NO_3)_2 \cdot 3H_2O$ (24.2 mg, 0.10 mmol) and 2-nitroimidazole (22.6 mg, 0.20 mmol) were dissolved in DMF (3.0 mL) in a 8 mL vial. After adding 0.2 mL of 0.5 M HNO_3 aqueous solution, the vial was capped and tightly sealed with a Teflon tape, and heated in a temperature-fixed oven at 45 °C for 16 hours. As soon as the reaction finishes, produced greenish-blue crystals were filtered and washed with DMF (3 mL × 3) and diethyl ether (3 mL × 3). The washed crystals were immersed in diethyl ether (3 mL) followed by evacuation in vacuum for 1 day at room temperature. The yield was 11.2% based on 1 mole of $Cu(NO_3)_2 \cdot 3H_2O$. Elemental microanalysis for the evacuated $Cu(nIm)_2$ = $C_6H_4N_6O_4Cu$: Calcd.: 25.05; H, 1.40; N, 29.22 %. Found: 25.05; H, 1.40; N, 29.22 %.

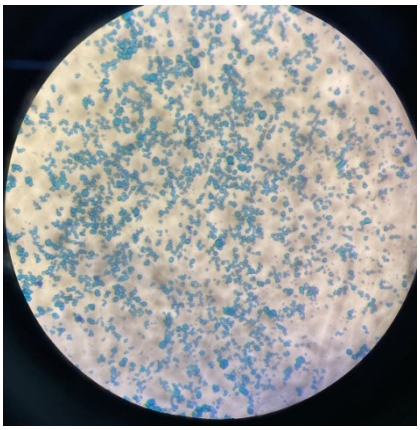

Fig. S8. An optical microscope image of Cu-ZIF-**rho** crystals.

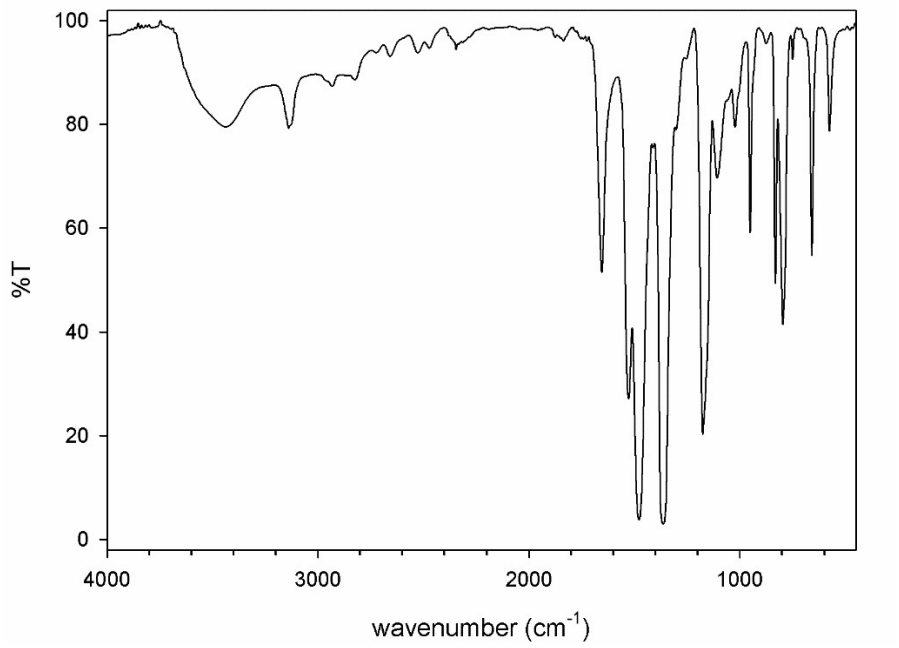

Fig. S9. The IR spectrum of the microcrystalline Cu-ZIF-**rho.**

The formula of the as-synthesized Cu-ZIF-**rho** was $[Cu(nIm)_2]\cdot(DMF)_{1.86}$ based on the ^{1}H-NMR analysis as follows. The as-synthesized Cu-ZIF-**rho** crystals were scattered on a filter paper, and cyclohexane was poured onto the crystals to wash out the DMF solvent on the crystal surfaces. Then, the crystals were dried in air for about 2 min until the crystals became free-running. The surface-dried crystals were quickly put in an NMR tube and dissolved with DCl (20 µL)/DMSO-d_6 (0.5 mL). In the spectrum, the molar ratio between 2-nitroimidazole (*a*) and DMF (*b* + *c* + *d*) was 2.00:1.86 calculated with the integration of their signals (Fig. S14).

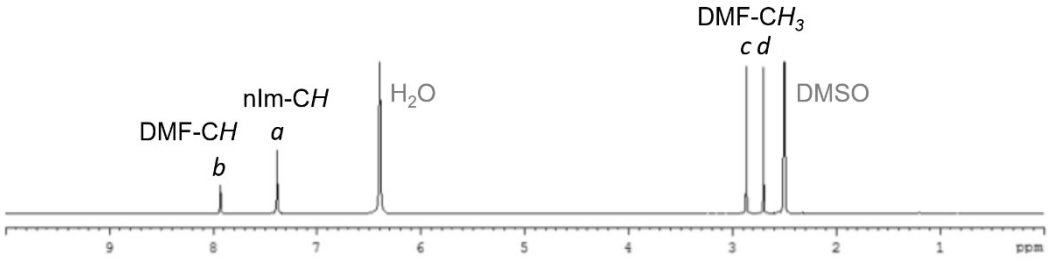

Fig. S10. The ^{1}H-NMR spectrum of the as-synthesized Cu-ZIF-**rho** crystals with δ 7.93 (s, 0.4543), 7.39 (s, 1.0000), 2.87 (s, 1.4005), 2.70 (s, 1.4062), where the numbers in the parentheses are the peak integration values.

Sub-micron crystals (Method B). When $Cu(NO_3)_2\cdot3H_2O$ (24.2 mg, 0.10 mmol), 2-nitroimidazole (22.6 mg, 0.20 mmol), and imidazole (6.81 mg, 0.10 mmol) were dissolved together in DMF (3.0 mL) at room temperature in an 8 mL vial, greenish-blue solids began to precipitate. The reaction mixture was standing on a bench for 1 h until the precipitate naturally settled to the bottom of the vial. The precipitate was filtered and washed with neat DMF (3 mL × 3) and immersed in diethyl ether (3 mL).

After 1 day, the solid was filtered and washed with diethyl ether (3 mL × 3), and dried under reduced pressure for 1 day. The yield was 28.6 % based on 1 mole of $Cu(NO_3)_2 \cdot 3H_2O$. The particle size was ca. 500 nm based (Fig. S15). Elemental microanalysis for the evacuated $Cu(nIm)_2$ = $C_6H_4N_6O_4Cu$: Calcd.: 25.05; H, 1.40; N, 29.22 %. Found: 25.17; H, 1.40; N, 29.00 %.

The phase purity was also confirmed by measuring PXRD patterns (Fig. S16).

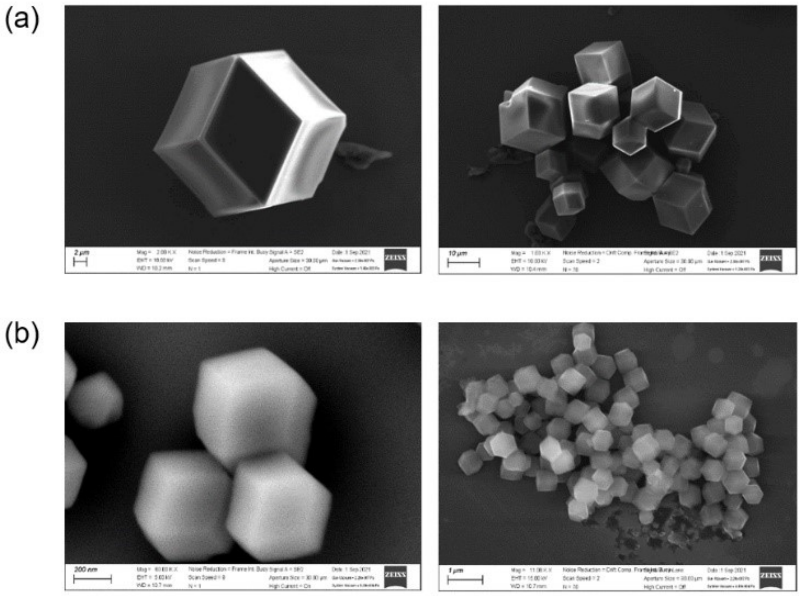

Fig. S11. SEM images of Cu-ZIF-**rho** rhombic dodecahedron crystals prepared by (a) Method A and (B) Method B, respectively. The average size of the crystals is (a) ca. 10 μm and (b) 500 nm, respectively.

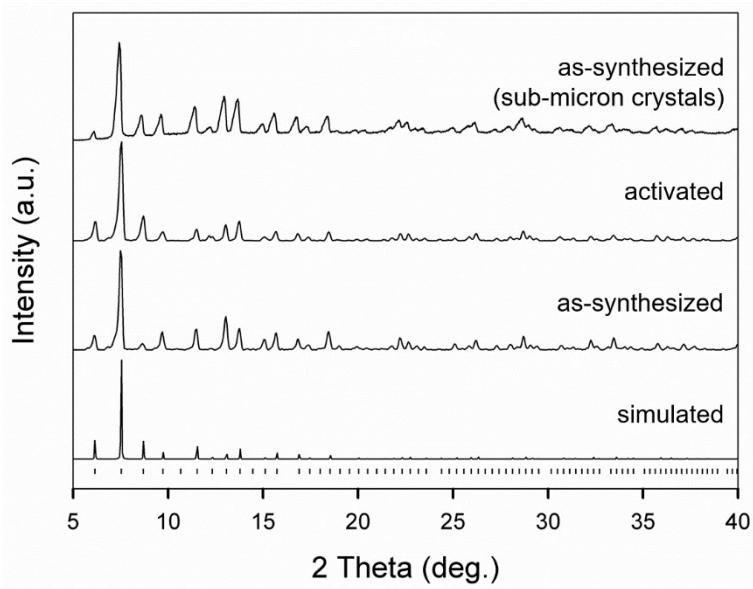

Fig. S12. The measured and simulated PXRD patterns for Cu-ZIF-**rho**. The activated sample was obtained by heating Cu-ZIF-**rho** at 160 °C for 10 h.

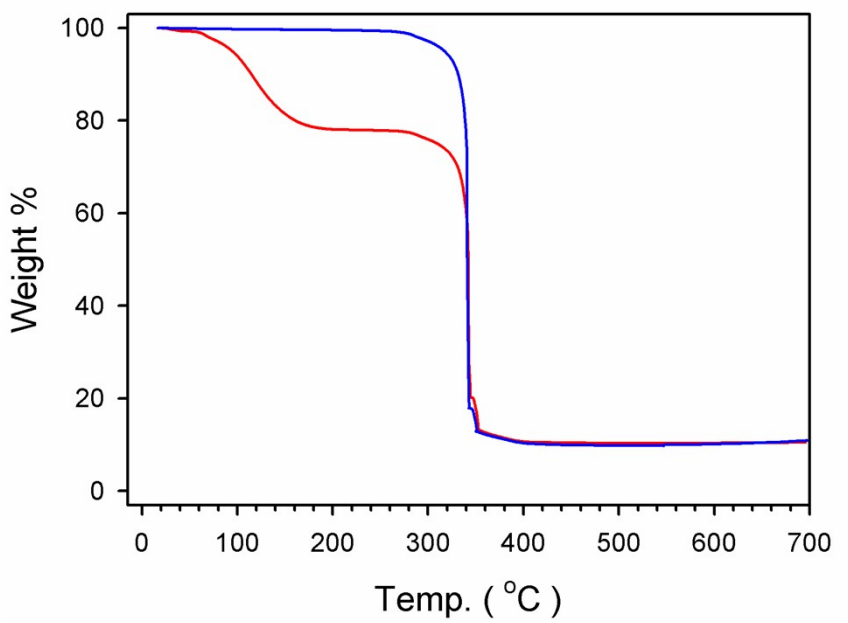

Fig. S13. The TGA thermograms of as-synthesized and activated Cu-ZIF-**rho** heat at 5 °C/min in air, respectively.

2.3. Cu-ZIF-**sql**

Single crystals. DMF (5.0 mL), NMP (5.0 mL), and MeOH (1.0 mL) were mixed and bubbled with N_2 gas for 30 min. In an 8 mL vial, CuCl (9.9 mg, 0.1 mmol) and IcaH (16.8 mg, 0.2 mmol) were placed together with 2.2 mL of the mixed solvent. The vial was tightly capped and heated in an oven at 85°C for 3 days, and only a few small light violet crystals were serendipitously obtained along with unidentified black solids; despite many attempts, the reaction could not be reproduced.

Section 3. Chemical Stability Tests in Aqueous Solutions at pH = 2 - 12

To investigate the chemical stability of Cu-ZIF-**gis** and Cu-ZIF-**rho**, 10 mg of each Cu-ZIF sample was immersed in 5.0 mL of HCl (pH = 2 – 6) or NaOH (pH = 8 – 12) aqueous solution for seven days at room temperature. For the pH = 7 solutions, just distilled water was used. Both the Cu-ZIF-**gis** and Cu-ZIF-**rho** crystals in the pH = 2 solutions were completely dissolved. In the cases of pH =12 solutions, the color of the crystals changed to dark brown and the solution also became pale greenish-yellow for both the Cu-ZIFs. However, the measured PXRD patterns showed that the collected Cu-ZIF crystals from the pH = 12 solutions kept the original crystallinity except for the appearance of two broad peaks at 2θ = 35° ~ 40° for Cu-ZIF-**rho**.

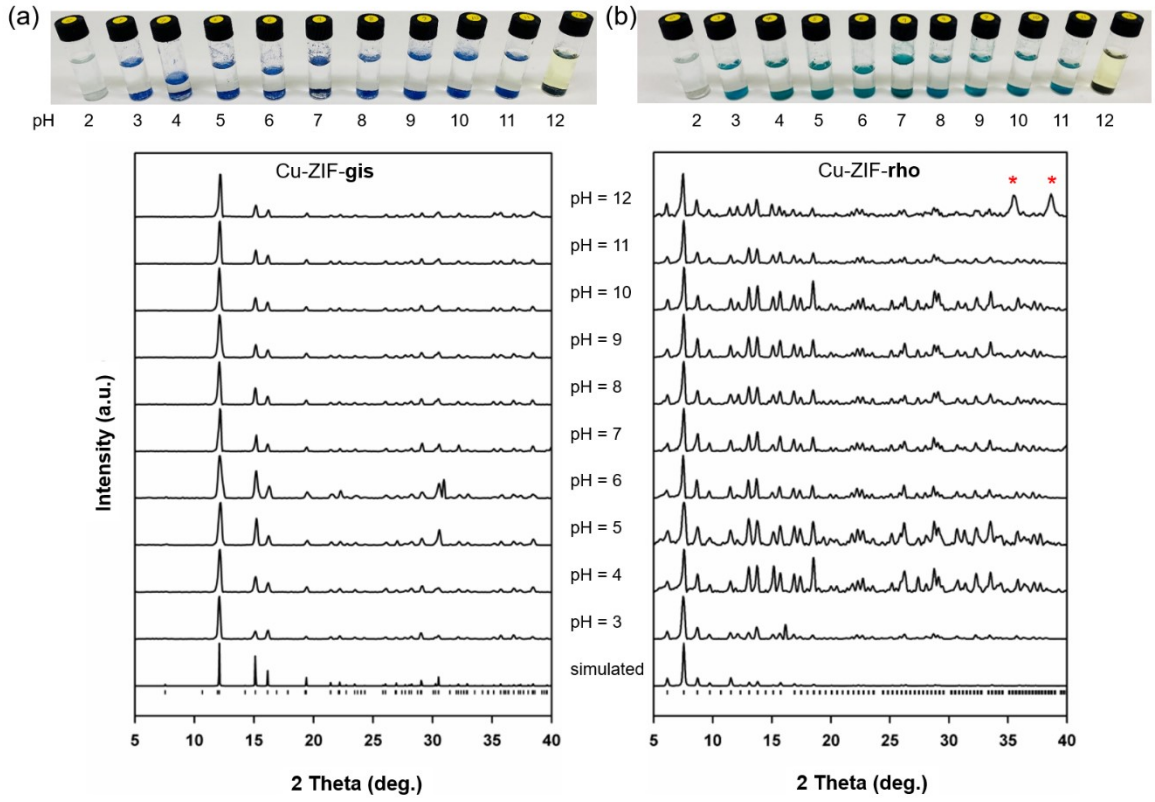

Fig. S14. PXRD patterns for the (a) Cu-ZIF-**gis** and (b) Cu-ZIF-**rho** samples. The samples were respectively collected from the aqueous solutions (pH = 2 – 12) after seven days at room temperature. The observed broad and intense peaks (*) for the Cu-ZIF-**rho** at pH = 12 are ascribed to CuO (002, 11-1) and (111, 200) reflections, respectively.

Table S1. ICP analysis results for the selected Cu-ZIF samples in aqueous solution in **Fig. S14**. The ICP analysis was conducted using a Perkin Elmer NexION 2000 at the Analysis Center of Kyungpook National University. Following the filtering of the sample solution through a syringe filter with a pore size of 0.45 μm, 1.0 mL of each aqueous solution was diluted 25-fold.

Aqueous solution samples		Concentrations of Cu(II) in aqueous solutions by ICP analysis (atomic weight of Cu = 63.546)			Calculated Cu(II) concentrations of the initial Cu-ZIF sample (f.w. of $Cu(nIm)_2$ = 287.69)		Dissolved portion of Cu(II) in aqueous solutions
		μg/L[a]	mg/L	mmol/L	mg/L[b]	mmol/L	%
Cu-ZIF-**gis**	pH = 3	3177	3.18	0.050	2000	6.95	0.72
	pH = 4	911	0.91	0.014	2000	6.95	0.21
	pH = 10	436	0.44	0.007	2000	6.95	0.10
	pH = 11	506	0.51	0.008	2000	6.95	0.11
Cu-ZIF-**rho**	pH = 3	3674	3.67	0.058	2000	6.95	0.83
	pH = 4	428	0.43	0.007	2000	6.95	0.10
	pH = 10	232	0.23	0.004	2000	6.95	0.05
	pH = 11	698	0.70	0.011	2000	6.95	0.16

[a] Raw data were multiplied by a dilution factor of 25.

[b] The initial mass of the Cu-ZIF sample in each vial is 10 mg/5 mL, which is converted to 2000 mg/L.

Section 4. Crystal Structure Analyses

A crystal was attached to an oil-covered CryoLoop on a goniometer head. Under a liquid nitrogen stream, the crystal was mounted on a Bruker diffractometer with an ADSC Q210 CCD area detector at 2D SMC with a silicon (111) double-crystal monochromator at Pohang Accelerator Laboratory (PAL). The wavelength of the X-ray generated by PLSII 2D bending magnets was adjusted to λ = 0.70000 Å. Data collection was conducted by an omega-scan method at 100K, 223 K and 298 K (Cu-ZIF-**gis**), 173 K (Cu-ZIF-**rho**), and 100 K (Cu-ZIF-**sql**), respectively. Over the range of the omega angle, 180°, diffraction images were collected with a step increase of 1° and an exposure time of 1 sec per frame at a detector distance of 90.00 mm, which was controlled using the PAL ADSC Quantum-210 ADX Program.[S1] The HKL3000sm (Ver. 703r) software package[S2] was used for the refinement of unit cell parameters and data reduction with a body-centered cubic unit cell. Absorption and decay corrections were applied. The structure was solved by direct methods using the SHELX-S program and further developed with difference Fourier syntheses, and subsequent refinement processes using the SHELX-L Version 2018/3.[S3] All non-hydrogen atoms were refined anisotropically, and hydrogen atoms were generated and refined using a riding model, HFIX with U values at 1.2 times the equivalent isotropic U of the atoms to which they are attached.

In the case of Cu-ZIF-**sql**, the TWIN -1 0 0 0 -1 0 0 0 -1 2 and BASF instructions in SHELX-L were used for further refinements; the final BASF parameter was 0.63976. Due to the solvent disorder in Cu-ZIF-**rho**, the SQUEEZE routine in the PLATON software package was used for the final stages of the structure refinement.[S4] Using the *fab*, *hkl*, and *res* files obtained from the PLATON SQUEEZE calculations, further refinement calculations using the ABIN instruction[S5] were conducted. CCDC deposition numbers are 2150501 (Cu-ZIF-**sql**), 2217784 (Cu-ZIF-**gis** at 100 K), 2150502 (Cu-ZIF-**gis** at 223 K), 2175590 (Cu-ZIF-**gis** at 298 K), and 2150503 (Cu-ZIF-**rho**), respectively.

Table S2. Crystal data and refinement results for Cu-ZIF-**sql**. **CCDC 2150501**

Empirical formula	$C_8 H_6 N_4 O_2 Cu$	Formula weight	253.71
Temperature	100(2) K	Wavelength	0.700 Å
Crystal system	Orthorhombic	Space group	*Aba*2 (No. 41)
Unit cell dimensions	a = 7.9150(16) Å	b = 13.333(3) Å	c = 8.8132(18) Å
	α = 90°	β= 90°	γ = 90°
Volume	930.1(3) Å^3	Z	4
Density (calculated)	1.812 g/cm^3	Absorption coefficient	2.240 mm^{-1}
F(000)	508	Crystal size	0.058 × 0.043 × 0.023 mm^3
θ Range for data collection	3.009 to 24.305°	Index ranges	$-9 \leq h \leq 9$, $-15 \leq k \leq 15$, $-9 \leq l \leq 9$
Reflections collected	1589	Independent reflections	629 [R(int) = 0.0447]
Completeness to θ = 24.835°	85.1 %	Absorption correction	Empirical
Max. and min. transmission	1.000 and 0.829	Refinement method	Full-matrix least-squares on F^2
Data / restraints / parameters	629 / 1 / 70	Goodness-of-fit on F^2	1.158
Final R indices [I>2σ(I)]	R1 = 0.0763, wR2 = 0.2348	R indices (all data)	R1 = 0.0823, wR2 = 0.2484
BASF twin parameters	0.64(17), 0.36(17)	Extinction coefficient	n/a
Largest diff. peak and hole	1.747 and -1.405 e.Å^{-3}		

Table S3. Selected Bond distances [Å] and angles [°] for Cu-ZIF-**sql**.

Cu1–N1	1.993(15)	Cu1–N1^a	1.993(15)	Cu1–N2^b	2.004(15)	Cu1–N2^c	2.004(15)
Cu1–O1	2.594(8)	Cu1–O1^a	2.594(8)				
N1–Cu1–N1^a	87.2(9)	N1^a –Cu1–N2^b	89.3(4)	N1–Cu1–N2^c	89.3(4)	N2^b –Cu1–N2^c	94.6(9)
N1–Cu1–N2^b	173.5(5)	N1^a –Cu1–N2^c	173.5(5)				
O1^a –Cu1–O1	153.4(7)						

Symmetry transformations used to generate equivalent atoms: a) -x+1, -y+1, z; b) x+1/2, -y+1, z+1/2; c) -x+1/2, y, z+1/2.

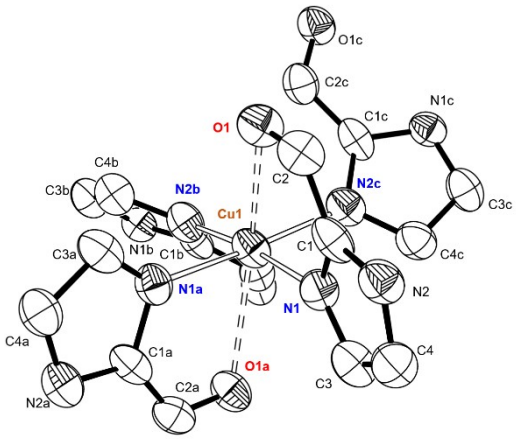

Fig. S15. ORTEP drawing of the coordination sphere of Cu-ZIF-**sql** with thermal ellipsoids at a 50% probability level. The atoms labeled with trailers are generated by symmetry operations: a) -x+1, -y+1, z; b) x+1/2, -y+1, z+1/2; c) -x+1/2, y, z+1/2. H atoms are not drawn for simplicity.

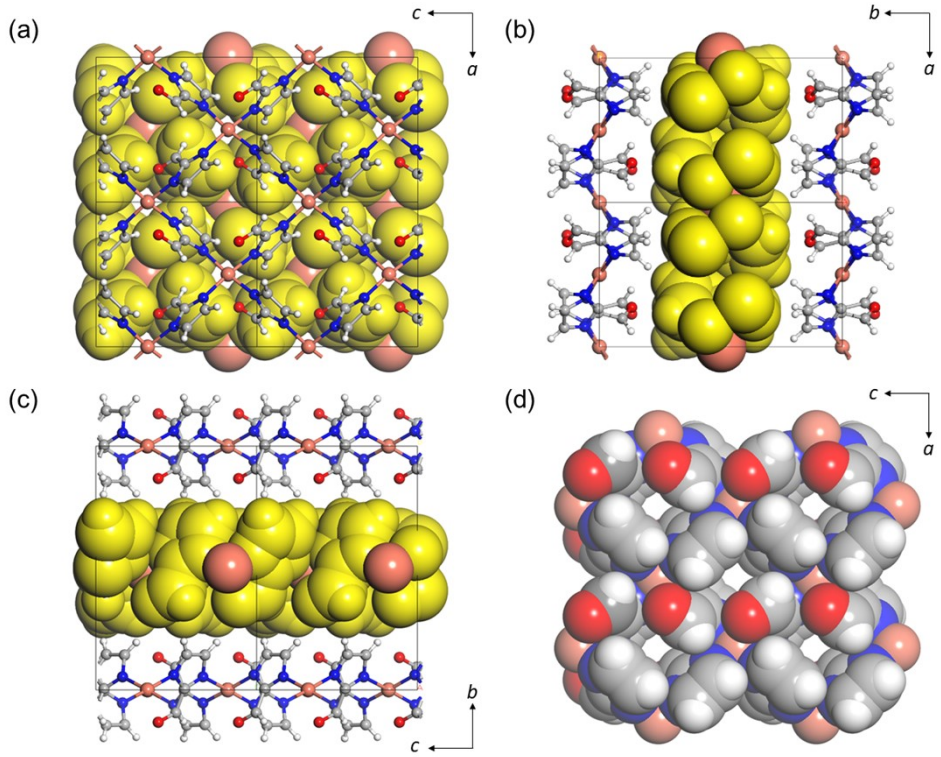

Fig. S16. Packing diagrams of Cu-ZIF-**sql** along (a) the *b*-, (b) *c*-, and (d) *a*-axis, respectively. The yellow-colored middle layer is displayed with a space-filling model, where Cu atoms are shown with brown spheres. (d) A space-filling drawing of the edge-sharing 4MRs in the top layer in (a).

Table S4a. Crystal data and refinement results for Cu-ZIF-**gis** at 100 K. **CCDC 2217784**

Empirical formula	$C_6 H_4 N_6 O_4 Cu$	Formula weight	287.69
Temperature	100(2) K	Wavelength	0.700 Å
Crystal system	Tetragonal	Space group	$I4_1md$ (No. 109)
Unit cell dimensions	a = 23.392(3) Å	b = 23.392(3) Å	c = 7.6930(15) Å
	α = 90°	β= 90°	γ = 90°
Volume	4209.5(14) $Å^3$	Z	16
Density (calculated)	1.816 g/cm^3	Absorption coefficient	2.009 mm^{-1}
F(000)	2288	Crystal size	0.053 × 0.035 × 0.010 mm^3
θ Range for data collection	2.425 to 27.779°	Index ranges	-31≤ h ≤31, -21≤ k ≤22, -10≤ l ≤10
Reflections collected	5016	Independent reflections	2753 [R(int) = 0.0948]
Completeness to θ = 24.835°	99.2 %	Absorption correction	Empirical
Max. and min. transmission	1.000 and 0.451	Refinement method	Full-matrix least-squares on F^2
Data / restraints / parameters	2706 / 1 / 160	Goodness-of-fit on F^2	1.030
Final R indices [I>2σ(I)]	R1 = 0.0339, wR2 = 0.0912	R indices (all data)	R1 = 0.0350, wR2 = 0.0923
Absolute structure parameter	0.015(10)	Extinction coefficient	n/a
Largest diff. peak and hole	0.402 and -1.131 e.$Å^{-3}$		

Table S4b. Crystal data and refinement results for Cu-ZIF-**gis** at 223 K. **CCDC 2150502**

Empirical formula	$C_6 H_4 N_6 O_4 Cu$	Formula weight	287.69
Temperature	223(2) K	Wavelength	0.700 Å
Crystal system	Tetragonal	Space group	$I4_1md$ (No. 109)
Unit cell dimensions	a = 23.426(3) Å	b = 23.426(3) Å	c = 7.7010(15) Å
	α = 90°	β= 90°	γ = 90°
Volume	4226.1(14) $Å^3$	Z	16
Density (calculated)	1.809 g/cm^3	Absorption coefficient	2.001 mm^{-1}
F(000)	2288	Crystal size	0.050 × 0.045 × 0.040 mm^3
θ Range for data collection	1.712 to 27.814°	Index ranges	-31≤ h ≤31, -31≤ k ≤31, -10≤ l ≤10
Reflections collected	17808	Independent reflections	2753 [R(int) = 0.0948]
Completeness to θ = 24.835°	100.0 %	Absorption correction	Empirical
Max. and min. transmission	1.000 and 0.954	Refinement method	Full-matrix least-squares on F^2
Data / restraints / parameters	2753 / 1 / 160	Goodness-of-fit on F^2	1.140
Final R indices [I>2σ(I)]	R1 = 0.0385, wR2 = 0.1170	R indices (all data)	R1 = 0.0401, wR2 = 0.1184
Absolute structure parameter	-0.010(8)	Extinction coefficient	n/a
Largest diff. peak and hole	1.259 and -0.907 e.$Å^{-3}$		

Table S4c. Crystal data and refinement results for Cu-ZIF-**gis** at 298 K. **CCDC 2175590**

Empirical formula	$C_6 H_4 N_6 O_4 Cu$	Formula weight	287.69
Temperature	298(2) K	Wavelength	0.700 Å
Crystal system	Tetragonal	Space group	$I4_1md$ (No. 109)
Unit cell dimensions	a = 23.439(3) Å	b = 23.439(3) Å	c = 7.7040(15) Å
	α = 90°	β= 90°	γ = 90°
Volume	4232.5(14) $Å^3$	Z	16
Density (calculated)	1.806 g/cm^3	Absorption coefficient	1.998 mm^{-1}

F(000)	2288	Crystal size	0.092 × 0.090 × 0.042 mm^3
θ Range for data collection	1.711 to 27.814°	Index ranges	-31≤ h ≤31, -21≤ k ≤22, -10≤ l ≤10
Reflections collected	5155	Independent reflections	2741 [R(int) = 0.0206]
Completeness to θ = 24.835°	99.1 %	Absorption correction	Empirical
Max. and min. transmission	1.000 and 0.578	Refinement method	Full-matrix least-squares on F^2
Data / restraints / parameters	2741 / 1 / 160	Goodness-of-fit on F^2	1.055
Final R indices [I>2σ(I)]	R1 = 0.0202, wR2 = 0.0579	R indices (all data)	R1 = 0.0206, wR2 = 0.0581
Absolute structure parameter	0.008(6)	Extinction coefficient	n/a
Largest diff. peak and hole	0.256 and -0.468 e.Å^{-3}		

Table S5a. Selected Bond distances [Å] and angles [°] for Cu-ZIF-**gis** at 223 K.

Cu1–N1	1.988(3)	Cu1–N4	1.991(3)	Cu1–N2^a	1.990(2)	Cu1–N6	2.004(2)
Cu1–O4	2.762(2)	Cu1–O2^a	2.685(3)	Cu1–O1	2.928(3)	Cu1–O3	2.851(2)
N4–Cu1–N6	90.3(1)	N1–Cu1–N2^a	89.7(1)	N4–Cu1–N2^a	94.2(1)	N1–Cu1–N6	92.2(1)
N1–Cu1–N4	160.8(1)	N2^a–Cu1–N6	160.9(1)				
O2^a–Cu1–O4	152.8(1)	O1–Cu1–O3	153.6(1)	O4-Cu1-O1	129.0(1)		

Symmetry transformations used to generate equivalent atoms: a) y-1/2, -x+1, z-1/4.

Table S5b. Selected Bond distances [Å] and angles [°] for Cu-ZIF-**gis** at 223 K.

Cu1–N1	1.988(4)	Cu1–N4	1.996(4)	Cu1–N2^a	1.996(3)	Cu1–N6	2.007(3)
Cu1–O4	2.783(3)	Cu1–O2^a	2.688(4)	Cu1–O1	2.944(4)	Cu1–O3	2.853(3)
N4–Cu1–N6	90.3(1)	N1–Cu1–N2^a	89.5(1)	N4–Cu1–N2^a	94.1(1)	N1–Cu1–N6	92.3(1)
N1–Cu1–N4	161.1(2)	N2^a–Cu1–N6	161.2(1)				
O2^a–Cu1–O4	152.9(1)	O1–Cu1–O3	153.6(1)	O4-Cu1-O1	128.8(1)		

Symmetry transformations used to generate equivalent atoms: a) y-1/2, -x+1, z-1/4.

Table S5c. Selected Bond distances [Å] and angles [°] for Cu-ZIF-**gis** at 298 K.

Cu1–N1	1.988(2)	Cu1–N4	1.995(2)	Cu1–N2^a	1.992(2)	Cu1–N6	2.007(2)
Cu1–O4	2.787(2)	Cu1–O2^a	2.691(2)	Cu1–O1	2.947(2)	Cu1–O3	2.851(2)
N4–Cu1–N6	90.2(1)	N1–Cu1–N2^a	89.8(1)	N4–Cu1–N2^a	94.1(1)	N1–Cu1–N6	92.1(1)
N1–Cu1–N4	161.1(1)	N2^a–Cu1–N6	161.2(1)				
O2^a–Cu1–O4	153.0(1)	O1–Cu1–O3	153.6(1)	O4-Cu1-O1	128.7(1)		

Symmetry transformations used to generate equivalent atoms: a) y-1/2, -x+1, z-1/4.

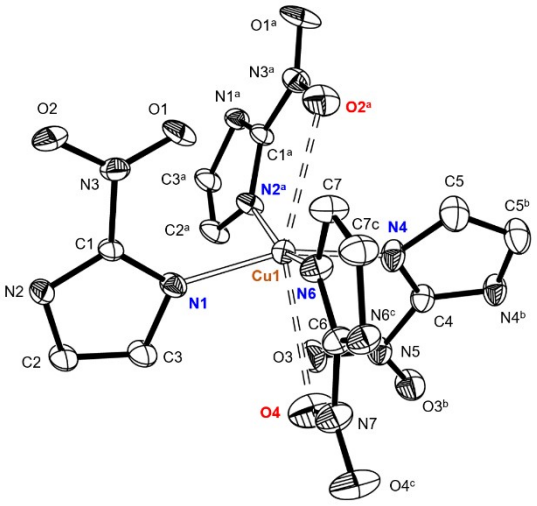

Fig. S17. ORTEP drawing of the coordination sphere of Cu-ZIF-**gis** at 223 K with thermal ellipsoids at a 50% probability level. The atoms labeled with trailers are generated by symmetry operations: a) y-1/2, -x+1, z-1/4; b) -x, y, z; c) x, -y+1, z. H atoms are not drawn for simplicity.

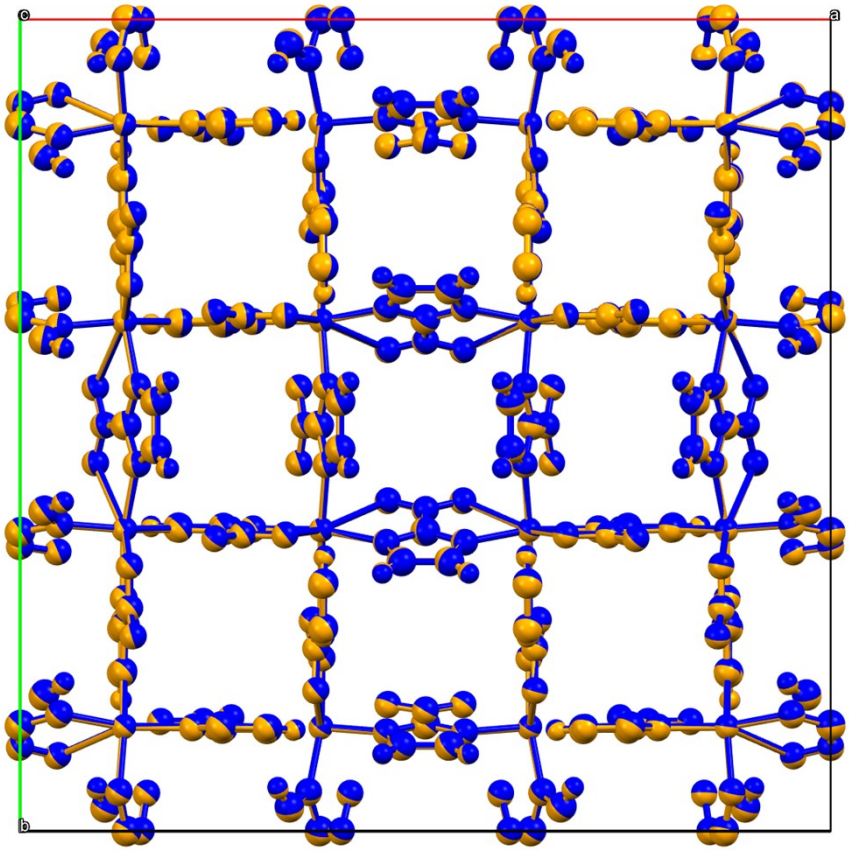

Fig. S18. Two crystal structures of Cu-ZIF-**gis** determined at 100 K (blue) and 298 K (orange), respectively, are overlaid.

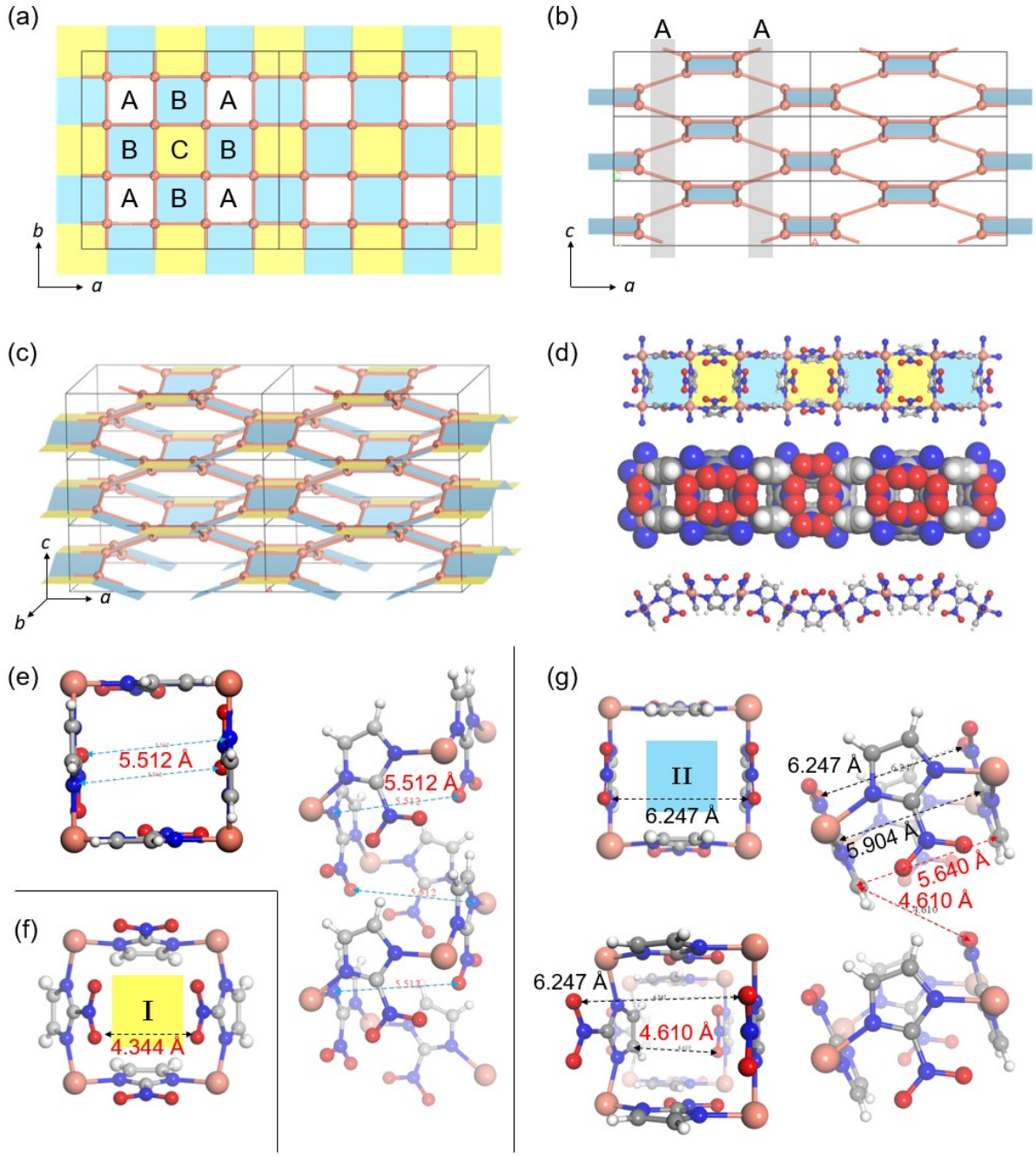

Fig. S19. (a) The GIS framework of Cu-ZIF-**gis** (223 K) is displayed with Cu^{2+} ions along the *c*-axis of the tetragonal unit cell. Two types of 4MRs are differentiated with yellow (type I) and blue (type II) colors, respectively, where the white squares are the crosssection of pore A and not 4MRs. (b) A projection view of the GIS network along the *b*-axis. (c) A slightly-tilted view of (b) shows the three-dimensional GIS framework compressed along the *c*-axis. (d) In 4MR chains, the blue-colored 4MRs are tilted while the yellow-colored ones are not. (e) The distance of 5.512 Å defines the free opening 2.442 Å of pore A. (f) The O···O distance of 4.344 Å defines the free opening 1.304 Å of pore C. (g) The 4MR units of pore B are tilted along the *c*-axis, giving a free opening of 1.390 Å.

Table S6. Crystal data and refinement results for Cu-ZIF-**rho** (after SQUEEZE). **CCDC 2150503**

Empirical formula	$C_6 H_4 N_6 O_4 Cu$	Formula weight	287.69
Temperature	173(2) K	Wavelength	0.700 Å
Crystal system	Cubic	Space group	*Im*-3*m* (No. 229)
Unit cell dimensions	a = 28.691(3) Å	b = 28.691(3) Å	c = 28.691(3) Å
	α = 90°	β= 90°	γ = 90°
Volume	23618(8) $Å^3$	Z	48
Density (calculated)	0.971 g/cm^3	Absorption coefficient	1.074 mm^{-1}
F(000)	6864	Crystal size	0.049 × 0.045 × 0.034 mm^3
θ Range for data collection	1.398 to 27.803°	Index ranges	-38≤ h ≤38, -27≤ k ≤27, -26≤ l ≤26
Reflections collected	9772	Independent reflections	2799 [R(int) = 0.0127]
Completeness to θ = 24.835°	99.7 %	Absorption correction	Empirical
Max. and min. transmission	1.000 and 0.509	Refinement method	Full-matrix least-squares on F^2
Data / restraints / parameters	2799 / 0 / 84	Goodness-of-fit on F^2	1.027
Final R indices [I>2σ(I)]	R1 = 0.0219, wR2 = 0.0667	R indices (all data)	R1 = 0.0237, wR2 = 0.0674
Absolute structure parameter	-0.010(8)	Extinction coefficient	n/a
Largest diff. peak and hole	0.314 and -0.411 e.$Å^{-3}$		

Our SQUEEZE calculations show 2736 electrons present in the pores, which is equivalent to 68.4 DMF molecules based on 40 DMF(C_3H_7NO) electrons. However, NMR analysis suggested 89.3 DMF molecules for Cu-ZIF-rho ($Cu(nIm)_2(DMF)_{1.86}$, Z = 48). Thus, SQUEEZE electron densities are lower than NMR methods. DMF solvent molecules in open pores may have evaporated during crystal mounting, or their electron densities may not be accurately reflected due to pore disorders.

Table S7. Selected Bond distances [Å] and angles [°] for Cu-ZIF-**rho**.

Cu1–N1	2.0055(9)	Cu1–N1[a]	2.0054(9)	Cu1–N3	1.9838(9)	Cu1–N3[a]	1.9838(9)
Cu1–O1	2.6394(8)	Cu1–O1[a]	2.6395(8)	Cu1–O2	2.9185(9)	Cu1–O2[a]	2.9184(9)
N3–Cu1–N3[a]	95.62(5)	N3–Cu1–N1[a]	93.23(3)	N3[a] –Cu1–N1	93.23(3)	N1[a] –Cu1–N1	91.42(5)
N3–Cu1–N1	151.84(3)	N3[a] –Cu1–N1[a]	151.84(3)				
O1-Cu1-O1[a]	137.18(3)	O1[a] -Cu1-O2 [a]	136.10(2)	O1-Cu1-O2	136.10(2)	O2[a]–Cu1-O2	136.22(4)

Symmetry transformations used to generate equivalent atoms: a) y+1/2, x-1/2, -z+3/2

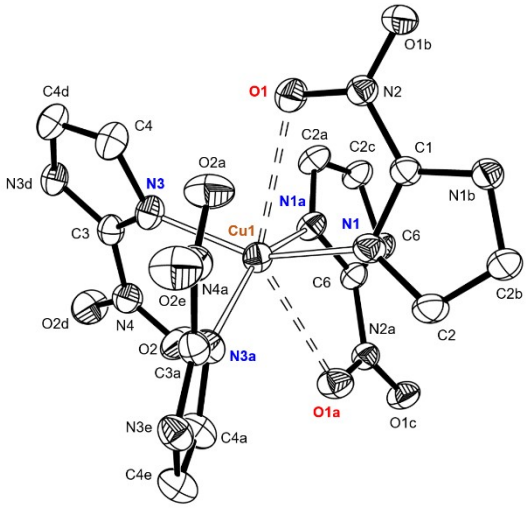

Fig. S20. ORTEP drawing of the coordination sphere of Cu-ZIF-**rho** with thermal ellipsoids at a 50% probability level. The atoms laebled with trailers are generated by symmetry operations: a) y+1/2, x-1/2, -z+3/2; b) x, -y+1, z; c) -y+3/2, x-1/2, -z+3/2; d) x, -z+1, -y+1; e) -z+3/2, x-1/2, y+1/2. H atoms are not drawn for simplicity.

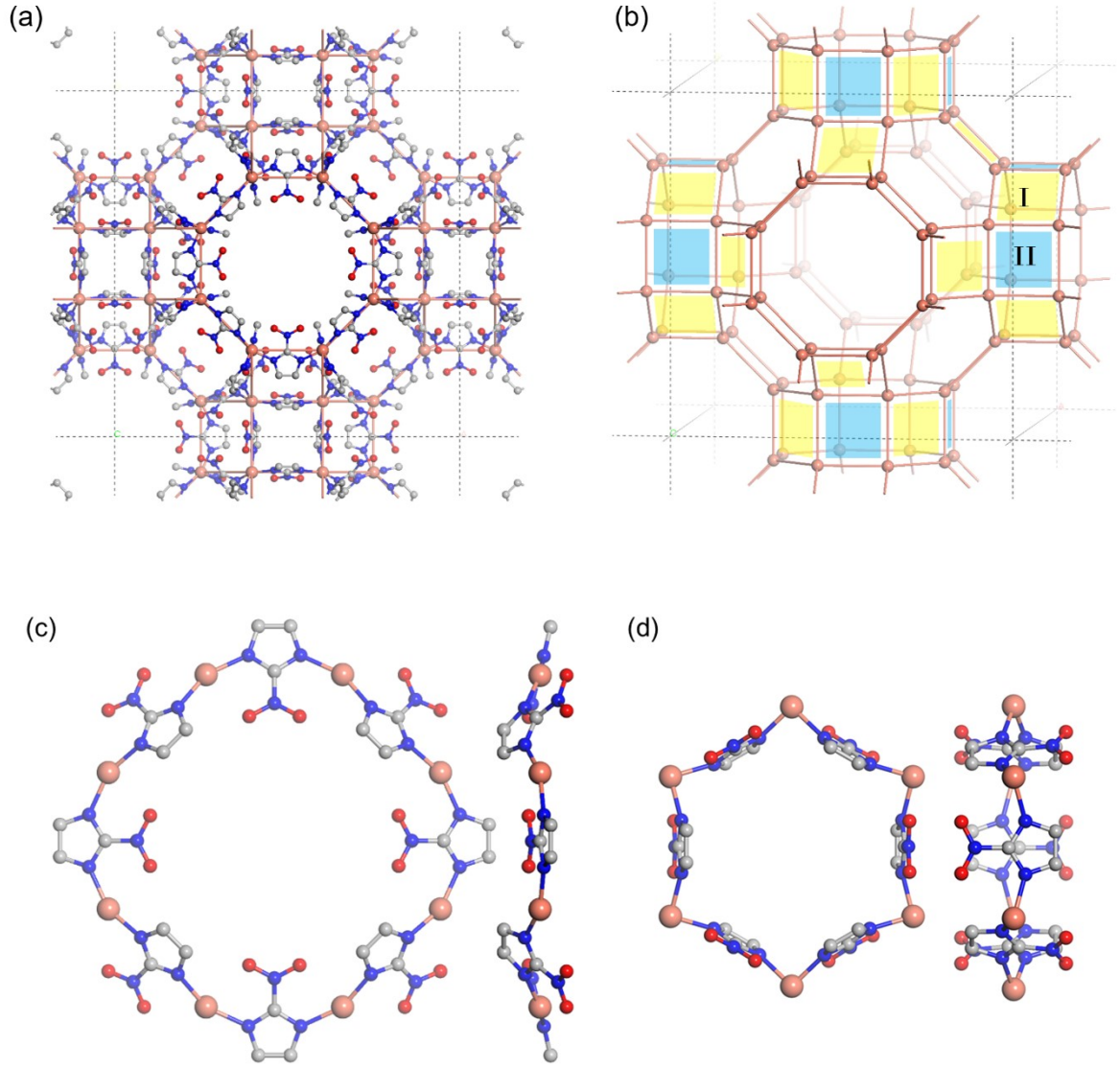

Fig. S21. (a) The framework of Cu-ZIF-**rho** is represented along the *c*-axis of a cubic unit cell. (b) The framework connectivity is simply represented with Cu^{2+} ions, where two types of 4MRs are highlighted with yellow (I) and blue (II) colors, respectively. Note that the I and II 4MRs share their edges or corners with 6MRs, respectively. (c) The front and side views of an 8MR and (d) a 6MR are displayed with ball-and-stick models, respectively, to show the relative orientations of the imidazolates. H atoms are not shown for simplicity.

Table S8. Angle distortion indices of selected ZIFs: DI = $[\sum_{i=1}^{6}|\Phi_i - \Phi_{avg}|]/(6\Phi_{avg})$ and RDI = DI/0.333.

ZIF	Net	Tetrahedral bond angles, Φ (∠N-M-N)							DI	RDI	Ref.
		Φ_1	Φ_2	Φ_3	Φ_4	Φ_5	Φ_6	Φ_{avg}			
(Square planar)	(D_{4h})	90.0	90.0	90.0	90.0	180.0	180.0	120.0	0.333	1.000	-
Cu-ZIF-**sql**	sql	87.2	89.3	89.3	94.6	173.5	173.5	117.90	0.314	0.943	this work
Cu-ZIF-**gis**	GIS	89.5	90.3	92.3	94.1	161.1	161.2	114.75	0.270	0.809	this work
Cu-ZIF-**rho**	RHO	91.4	93.2	93.2	95.6	151.8	151.8	112.86	0.230	0.691	this work
B	SOD	84.4	92.1	95.9	104.2	139.6	154.8	111.83	0.211	0.633	S6
G(avg.)	4,4L37								0.208	0.623	S6
		92.6	95.2	98.8	99.4	138.4	142.5	111.15	0.176		
		88.1	88.1	97.7	97.7	154.0	154.0	113.27	0.240		
O(avg.)	mog								0.204	0.611	S6
		94.1	95.2	98.3	98.3	140.8	140.8	111.24	0.177		
		92.4	92.6	93.3	94.8	146.3	157.3	112.78	0.231		
CdIF-9	RHO	95.9	95.9	100.6	105.9	131.9	131.9	110.33	0.130	0.391	S7
CdIF-8	SOD	99.9	99.9	99.9	99.9	131.1	131.1	110.28	0.126	0.378	S7
CoNIm(RHO)	RHO	98.2	99.6	99.6	104.5	129.4	129.4	110.12	0.116	0.350	S8
ZIF-74	GIS	98.7	104.6	108.8	108.9	113.0	122.9	109.51	0.052	0.155	S9
ZIF-68	GME	103.8	104.7	107.2	107.4	108.9	123.5	109.23	0.044	0.131	S9
ZIF-71	RHO	102.1	105.0	108.3	110.2	114.5	116.6	109.45	0.039	0.103	S9
ZIF-412(avg.)	ucb								0.039	0.118	S10
		99.6	105.7	107.6	108.6	113.3	121.2	109.34	0.048		
		103.9	105.0	105.3	111.4	112.4	118.3	109.37	0.042		
		104.2	108.0	108.2	108.3	113.3	114.5	109.42	0.027		
ZIF-300(avg.)	CHA								0.038	0.113	S11
		102.4	107.2	108.1	109.5	109.7	119.5	109.40	0.032		
		103.9	104.9	105.5	111.5	112.9	118.1	109.47	0.043		
ZIF-7	SOD	103.6	105.3	107.7	111.6	113.6	115.2	109.51	0.036	0.108	S12
CdIF-6	ANA	102.9	104.9	111.5	111.5	113.2	113.2	109.52	0.034	0.103	S7
ZIF-12	RHO	105.0	105.4	107.9	109.0	111.2	117.5	109.33	0.031	0.092	S12
ZIF-11	RHO	104.7	107.0	107.5	109.9	111.3	116.1	109.43	0.028	0.083	S12
CdIF-2	MER	104.6	105.4	110.1	110.6	111.2	115.1	109.49	0.028	0.083	S7
ZIF-20	LTA	104.7	106.4	108.3	110.5	111.1	115.5	109.44	0.027	0.081	S13
ZIF-6	GIS	107.6	107.7	107.7	109.1	109.1	115.4	109.43	0.018	0.054	S12
ZIF-3	DFT	107.1	107.5	108.1	110.0	111.4	112.5	109.44	0.017	0.051	S12
ZIF-10	MER	106.2	108.4	108.9	109.9	111.0	112.5	109.47	0.015	0.045	S12
ZIF-65	SOD	107.4	107.4	110.5	110.5	110.5	110.5	109.48	0.013	0.038	S9
CdIF-1	SOD	109.2	109.2	109.2	109.2	110.0	110.0	109.47	0.003	0.010	S7
ZIF-8	SOD	109.3	109.3	109.3	109.3	109.8	109.8	109.47	0.002	0.006	S12
(Tetrahedral)	(T_d)	109.5	109.5	109.5	109.5	109.5	109.5	109.47	0.000	0.000	-

Table S9. Internal angles of 4MRs for selected ZIFs.

ZIF	Net	4MR Internal angles, θ (∠N-M-N)					θ_{avg} /131.9°	Ref.
		θ_1	θ_2	θ_3	θ_4	θ_{avg}		
Cu-ZIF-**sql**	sql	87.15	89.35	89.35	94.64	90.12	0.68	this work
Cu-ZIF-**gis**	GIS	90.26	90.26	90.26	90.26	90.26	0.68	this work
		92.27	92.27	94.09	94.09	93.18	0.71	
Cu-ZIF-**rho**	RHO	91.42	91.42	91.42	91.42	91.42	0.69	this work
		93.23	93.23	93.23	93.23	93.23	0.71	
B	SOD	84.44	84.44	95.88	95.88	90.16	0.68	S6
G	4,4L37	-	-	-	-	-	-	S6
O	mog	98.30	98.30	98.35	98.35	98.33	0.75	S6
CdIF-9	RHO	100.63	100.63	100.63	100.63	100.63	0.76	S7
		131.87	131.87	131.87	131.87	131.87	1.00	
CdIF-8	SOD	131.13	131.13	131.13	131.13	131.13	0.99	S7
CoNIm(RHO)	RHO	98.24	98.24	98.24	98.24	98.24	0.74	S8
		129.36	129.36	129.36	129.36	129.36	0.98	
ZIF-74	GIS	122.93	122.93	122.93	122.93	122.93	0.93	S9
		108.84	108.84	108.92	108.92	108.88	0.83	
ZIF-68	GME	123.49	123.49	123.49	123.49	123.49	0.94	S9
		107.19	107.19	107.19	107.19	107.19	0.81	
		108.90	108.90	108.90	108.90	108.90	0.83	
ZIF-71	RHO	104.97	104.97	104.97	104.97	104.97	0.80	S9
		108.27	108.27	108.27	108.27	108.27	0.82	
		102.15	102.15	102.15	102.15	102.15	0.77	
ZIF-412	ucb	104.17	104.17	108.57	108.57	106.37	0.81	S10
		118.26	118.26	121.18	121.18	119.72	0.91	
		111.38	111.38	113.31	113.31	112.35	0.85	
ZIF-300	CHA	104.87	104.87	108.08	108.08	106.48	0.81	S11
		102.44	103.91	105.47	107.18	104.75	0.79	
ZIF-7	SOD	103.61	103.61	105.31	105.31	104.46	0.79	S12
CdIF-6	ANA	111.48	111.48	111.48	111.48	111.48	0.85	S7
ZIF-12	RHO	105.03	105.03	105.03	105.03	105.03	0.80	S12
		105.38	105.38	105.38	105.38	105.38	0.80	
		108.98	108.98	108.98	108.98	108.98	0.83	
ZIF-11	RHO	104.72	104.72	104.72	104.72	104.72	0.79	S12
		107.46	107.46	107.46	107.46	107.46	0.81	
		107.04	107.04	107.04	107.04	107.04	0.81	

Table S9. (Continued)

ZIF	Net	4MR Internal angles, θ (∠N-M-N)					θ_{avg} /131.9°	Ref.
		θ_1	θ_2	θ_3	θ_4	θ_{avg}		
CdIF-2	MER	111.23	111.23	111.40	111.40	111.32	0.84	S7
		109.82	109.82	110.12	110.12	109.97	0.83	
ZIF-20	LTA	104.73	104.73	104.73	104.73	104.73	0.79	S13
		110.54	110.54	110.54	110.54	110.54	0.84	
		106.42	106.42	106.42	106.42	106.42	0.81	
ZIF-6	GIS	115.39	115.39	115.39	115.39	115.39	0.88	S12
		107.73	107.73	107.73	107.73	107.73	0.82	
ZIF-3	DFT	110.04	110.04	110.04	110.04	110.04	0.83	S12
		107.51	107.51	107.51	107.51	107.51	0.82	
ZIF-10	MER	109.88	109.88	109.88	109.88	109.88	0.83	S12
		110.95	110.95	110.95	110.95	110.95	0.84	
ZIF-65	SOD	107.41	107.41	107.41	107.41	107.41	0.81	S9
CdIF-1	SOD	110.00	110.00	110.00	110.00	110.00	0.83	S7
ZIF-8	SOD	109.81	109.81	109.81	109.81	109.81	0.83	S12

Section 5. H_2 Adsorption Measurements for Cu-ZIF-**gis** at Low Temperature

5.1. H_2 and N_2 adsorption isotherms at 77 K

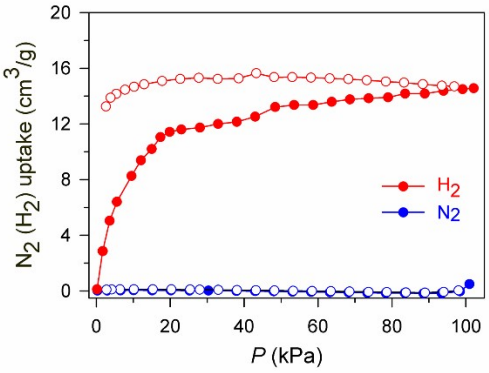

Fig. S22. N_2 and H_2 gas adsorption-desorption isotherms of Cu-ZIF-**gis** were measured at 77 K, respectively, using a BELSORP-mini (BEL-Japan, INC.). Filled and open circles represent the adsorption and desorption branches, respectively.

5.2. H_2 adsorption isotherms at 20 K – 150 K

The hydrogen adsorption isotherms of Cu-ZIF-**gis** from 150 K down to 20 K were further measured with a fully automated Sieverts apparatus (Autosorb-iQ2, Quantachrome Instruments) utilizing a temperature-controlled cryostat. Around 100 mg of the sample was activated at 160 ℃ under vacuum for 10 h. The temperature stability was less than 0.05 K during isotherm measurements at each temperature. Each isotherm measurement takes ca. 1~2 weeks.

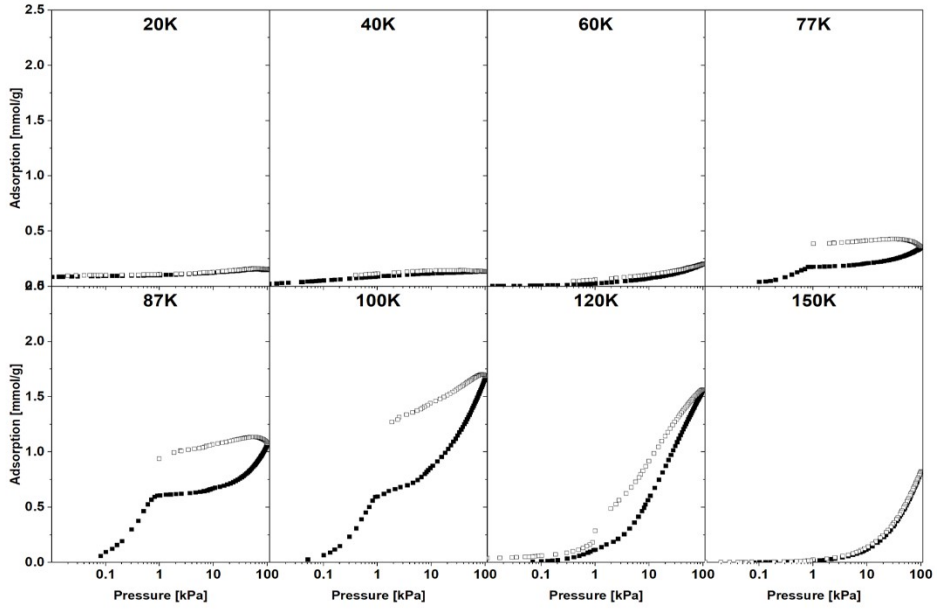

Fig. S23. High-resolution low-pressure hydrogen adsorption and desorption isotherms of Cu-ZIF-**gis** at various temperatures: 20 K, 40 K, 60 K, 77 K, 87K, 100 K, 120K, and 150 K. Closed and open symbols represent the absorption and desorption.

5.3. Thermal desorption spectra measurements of H_2

The thermal desorption spectrum of H_2 was performed in a home-built device with ca. 3.61 mg of Cu-ZIF-**gis** activated at 160 ℃ for 10 h under vacuum.[S14] The sample was exposed to H_2 atmosphere (1 bar) either at 20 K or RT, then rapidly cooled to 17 K. The unobserved residual gas molecules were removed by evacuation. Afterward, the sample was heated to 250 K with a linear heating rate of 6 K/min. The desorbed gas was continuously detected using a quadrupole mass spectrometer (QMS) and a pressure increase in the sample chamber. The area under the desorption peak is proportional to the desorbing amount of hydrogen, which can be quantified after careful calibration by TiH_2 of the TDS apparatus. We observed a weight change of 0.439% which corresponds to the storage of 2.187 mmol H_2 in 1.0 g of Cu-ZIF-**gis**.

A series of the thermal desorption spectra for the H_2-loaded Cu-ZIF-**gis** at 100 K with different heating rates made it possible to assess the H_2 desorption energy (Fig. S29). The desorption energy was determined by applying the Polanyi-Wigner equation to thermal desorption spectra.[S15] This method is based on the assumption that adsorption and desorption are reversible processes, and the desorption energy is independent of the coverage or temperature. A plot of $\ln\left(\frac{\beta}{T_{max}^2}\right)$ versus $1/T_{max}$ yields a straight line, and the desorption energy is determined from the slope.

$$\ln\left(\frac{\beta}{T_{max}^2}\right) = -\frac{E_{des}}{RT_{max}} + \ln\left(\frac{vR\theta_0}{E_{des}}\right)$$

(: coverage, β: heating rate, v: frequency factor, E_{des}: desorption energy, R: gas constant, T: temperature)

After exposure to 1 bar H_2 atmosphere at 100 K (30 min exposure time), the sample was cooled to 18 K. Then, the thermal desorption spectra were recorded by applying the different heating rates of 1 K/min, 3 K/min, 4.5 K/min, and 6 K/min. The determined desorption energy of hydrogen is 22.8 kJ/mol.

Section 6. Calculations of the Q_{st} values for Cu-ZIF-**gis**

Table S10. Selected Bond distances [Å] and angles [°] for Cu-ZIF-**rho**.

Fitting methods	-ΔH = Q_{st} (kJ/mol) at the H_2 loading amount of of 0.01 mmol/g	
	*Low pressure isotherms (120 K – 150 K)	High pressure isotherm (273 K – 298 K)
CC-DSFL	13.7	11.8
CC-FL	12.3	10.4
Virial	10.9	11.3

CC: Clausius-Clayperon
FL: Freundlich–Langmuir
DSFL: Dual-Site Freundlich–Langmuir
* Adsorption branches were selected for the calculations.

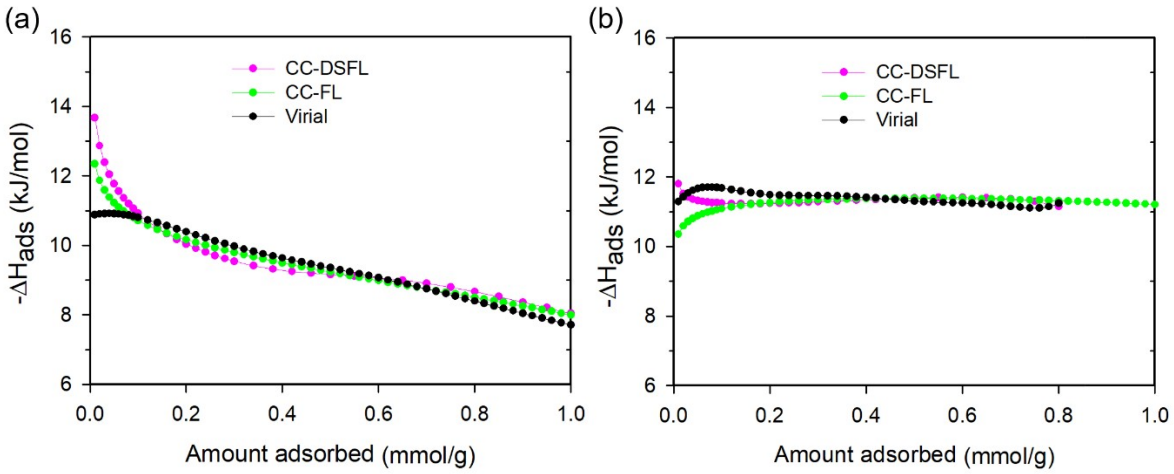

Fig. S24. Calculation of ΔH_{ads} using the H_2 adsorption isotherms on Cu-ZIF-**gis** (a) at 120K/150 K and (b) 273K/298 K, respectively.

Section 7. N_2 adsorption isotherms for Cu-ZIF-**rho**

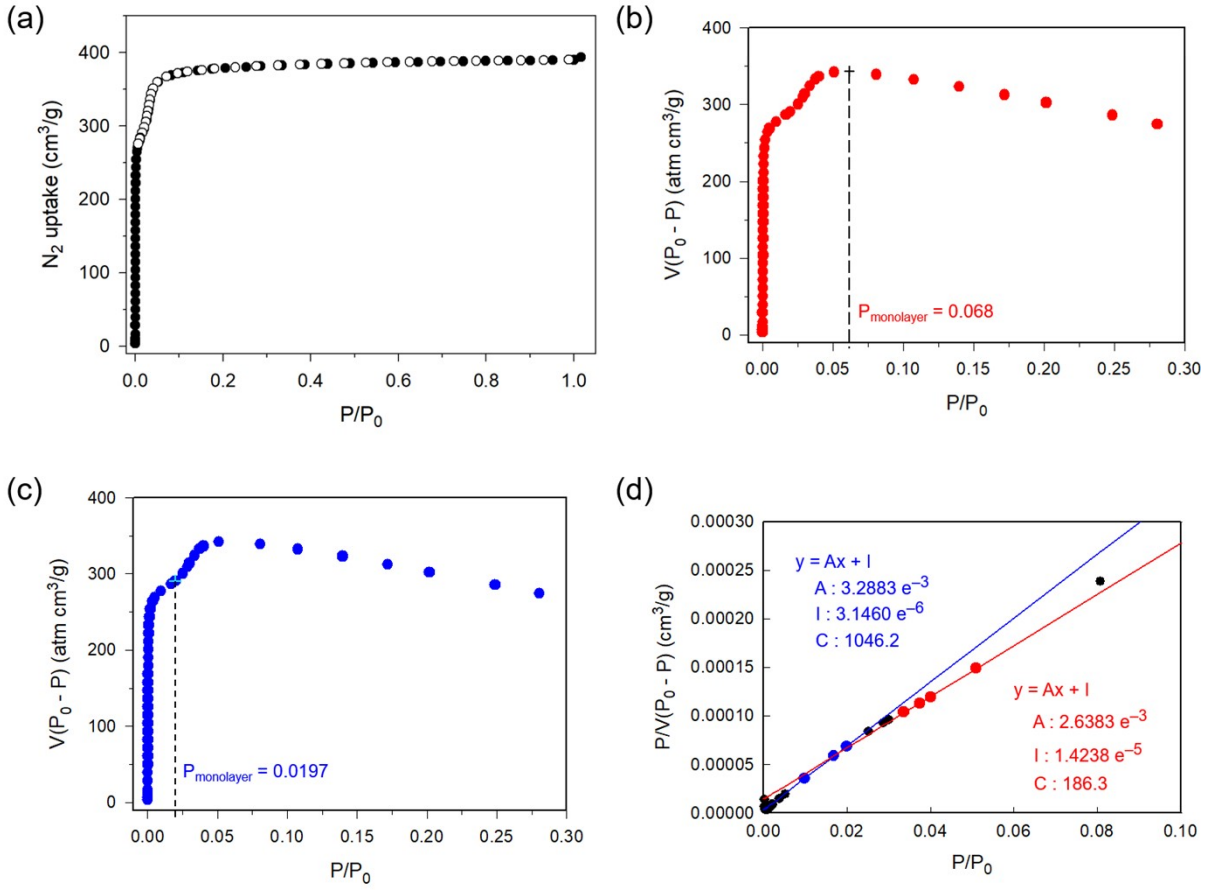

Fig. S25. BET analysis of Cu-ZIF-**rho** (Crystals). (a) N_2 gas adsorption-desorption isotherm measured at 77 K for Cu-ZIF-**rho**. The absorption branch is marked with filled circles. $V(P_0 - P)$ vs. P/P_0 plots have monolayer gas adsorption volumes of (b) 377.0 cm^3/g at $P/P_0 = 0.068$ and (c) 303.8 cm^3/g at $P/P_0 = 0.0197$, respectively. (d) Plots of the linear fitting below the monolayer pressures in (b) and (c), respectively. The fitting gives the BET surface areas of 1640.9 and 1322.4 m^2/g, respectively. The solvent surface of Cu-ZIF-**rho** was 3210.8 $Å^2$ per unit cell or 1400.2 m^2/g based on the calculated accessible surface area using BIOVIA Materials Studio[S16]; the radius of a used probe was 1.84 Å, half the kinetic diameter of N_2. [S17] Therefore, we have chosen 1322.4 m^2/g as the BET surface area of Cu-ZIF-**rho** because it is closer to the calculated geometric surface area.

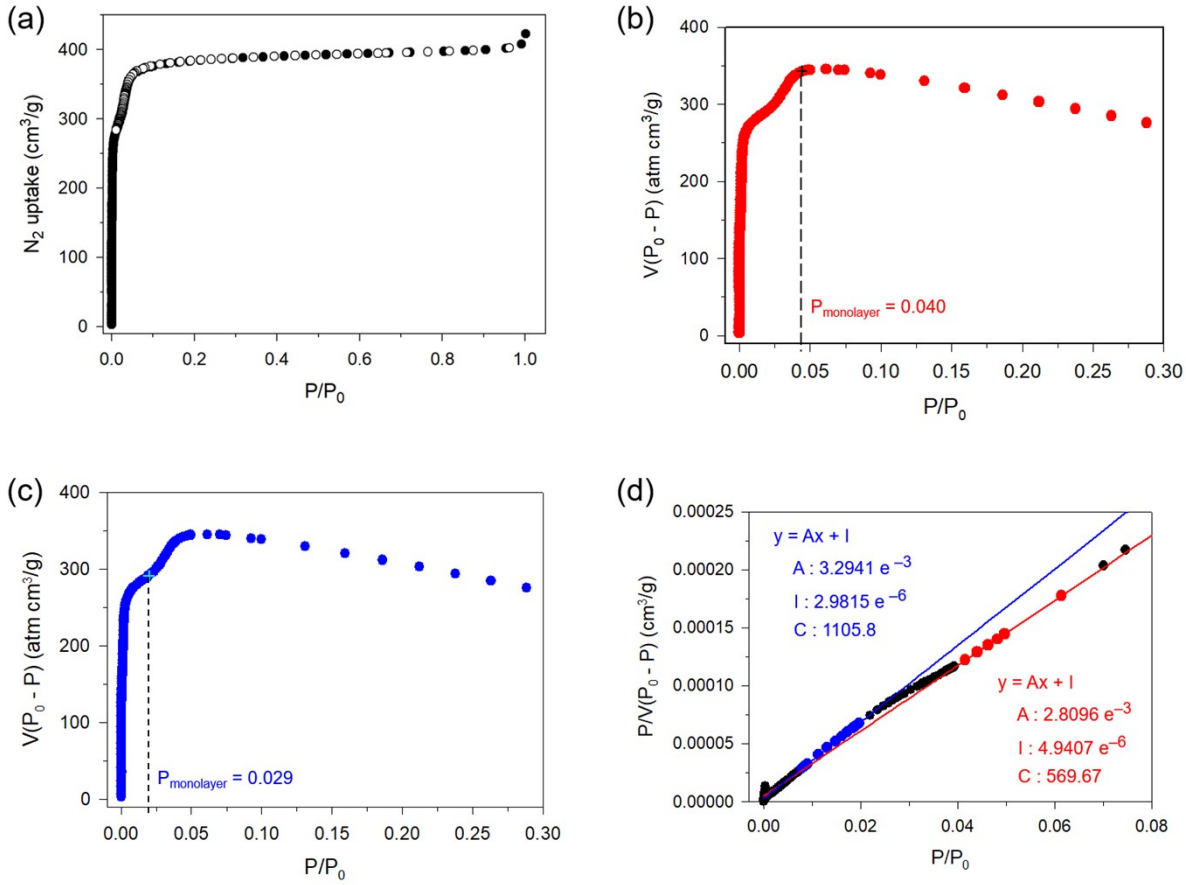

Fig. S26. BET analysis of Cu-ZIF-**rho** (Sub-micron crystals). (a) N_2 gas adsorption-desorption isotherm measured at 77 K for sub-micron crystalline Cu-ZIF-**rho**. The absorption branch is marked with filled circles. $V(P_0 – P)$ vs. P/P_0 plots have monolayer gas adsorption volumes of (b) 353.3 cm^3/g at $P/P_0 = 0.040$ and (c) 303.3 cm^3/g at $P/P_0 = 0.029$, respectively. (d) Plots of the linear fitting below the monolayer pressures in (b) and (c), respectively. The fitting gives the BET surface areas of 1546.4 and 1320.1 m^2/g, respectively. The solvent surface of Cu-ZIF-**rho** was 3210.8 $Å^2$ per unit cell or 1400.2 m^2/g based on the calculated accessible surface area using BIOVIA Materials Studio [S16]; the radius of a used probe was 1.84 Å, half the kinetic diameter of N_2.[S17] Therefore, we have chosen 1320.1 m^2/g as the BET surface area of sub-micron Cu-ZIF-**rho** because it is closer to the calculated geometric surface area.

Section 8. Gas Adsorption Measurements for Cu-ZIF-**rho**

Table S11. Gas adsorption enthalpy values at zero coverages and maximum uptakes of Cu-ZIF-**rho**.

Gas	$-\Delta H_{ads}$ (kJ/mol)		Amount adsorbed (cm^3/g, 1 bar)		
	Virial method [S18]	Clausius–Clapeyron eq. w/t Dual-site Langmuir-Freundlich correction [S18]			
H_2	9.0 (max. 9.3)	26.0 (77 K, 87 K)	85.9 (87K)	127.6 (77K)	
CH_4	15.3	15.4 (253 K, 273 K) 14.9 (253 K, 298 K) 15.2 (273 K, 273 K)	16.8 (253K)	12.1 (273K)	7.7 (298K)
CO_2	20.8	23.7 (253 K, 273 K) 22.8 (253 K, 273 K) 22.3 (253 K, 273 K)	88.6 (253K)	48.5 (273K)	24.4 (298K)

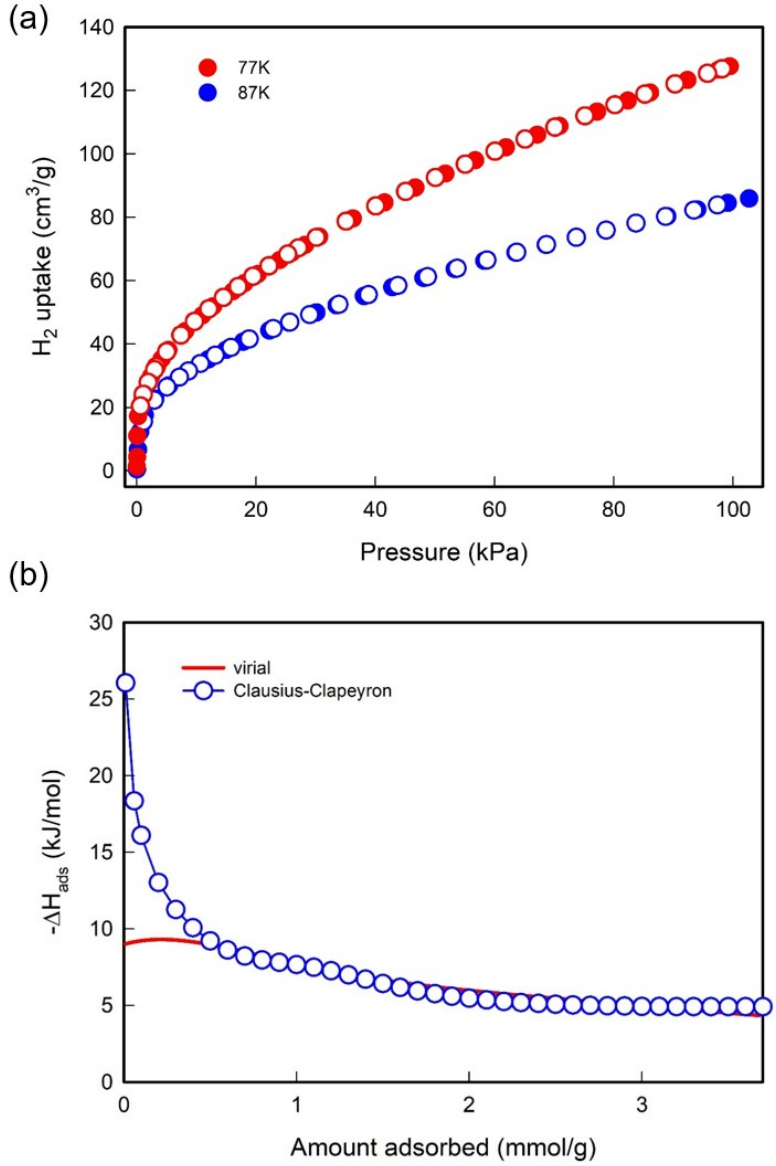

Fig. S27. H_2 adsorption on Cu-ZIF-**rho**. (a) H_2 gas adsorption-desorption isotherms measured at 77 K and 87 K, respectively. (b) Isosteric enthalpy plot of the H_2 adsorption from virial analysis and the DS-FL fit together with the Clausius–Clapeyron equation (DS-FL/CC) and the Virial analysis.[S18]

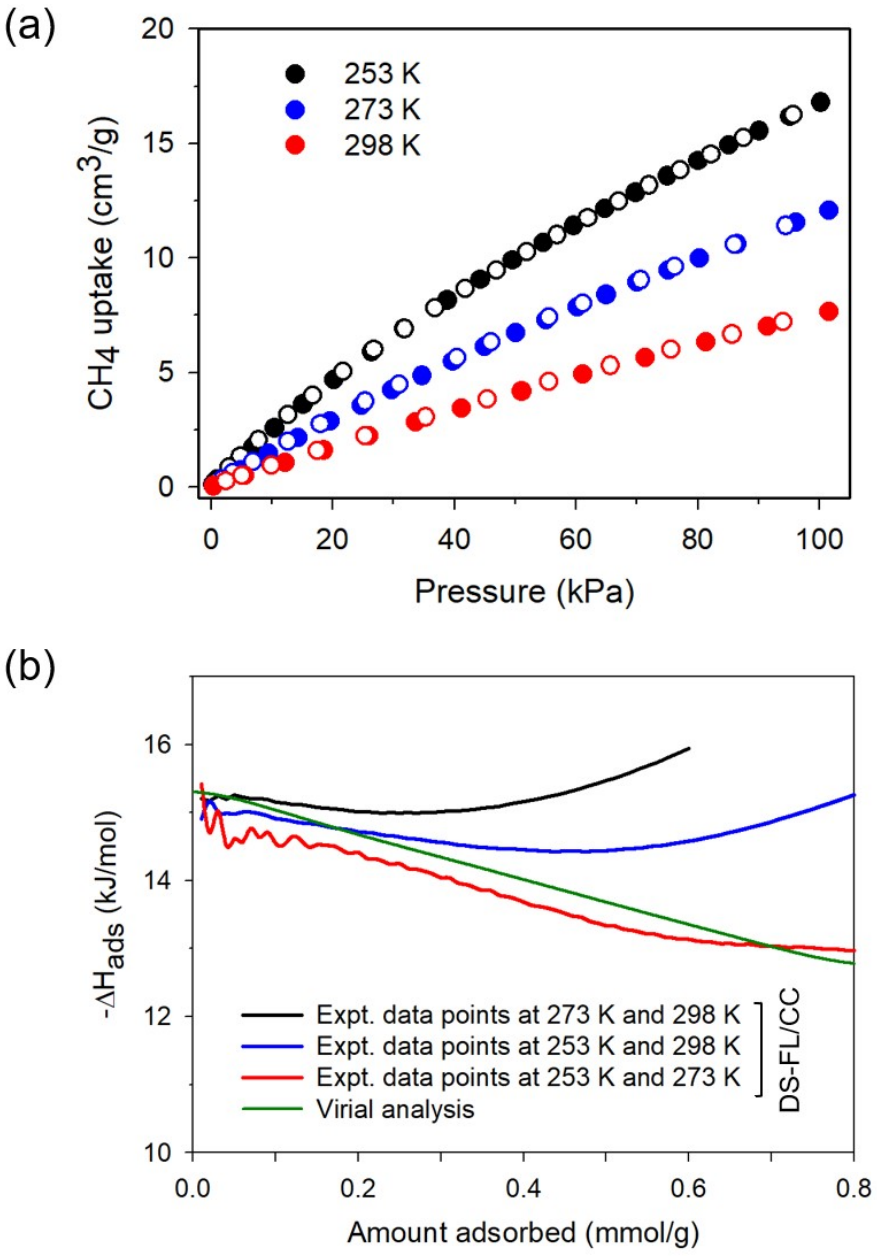

Fig. S28. CH_4 adsorption on Cu-ZIF-**rho**. (a) Measured CH_4 gas adsorption-desorption isotherms at three different temperatures, where the absorption branches are marked with filled circles. (b) Isosteric enthalpy plots of CH_4 adsorption from a DS-FL/CC method and the Virial analysis, respectively.[S18]

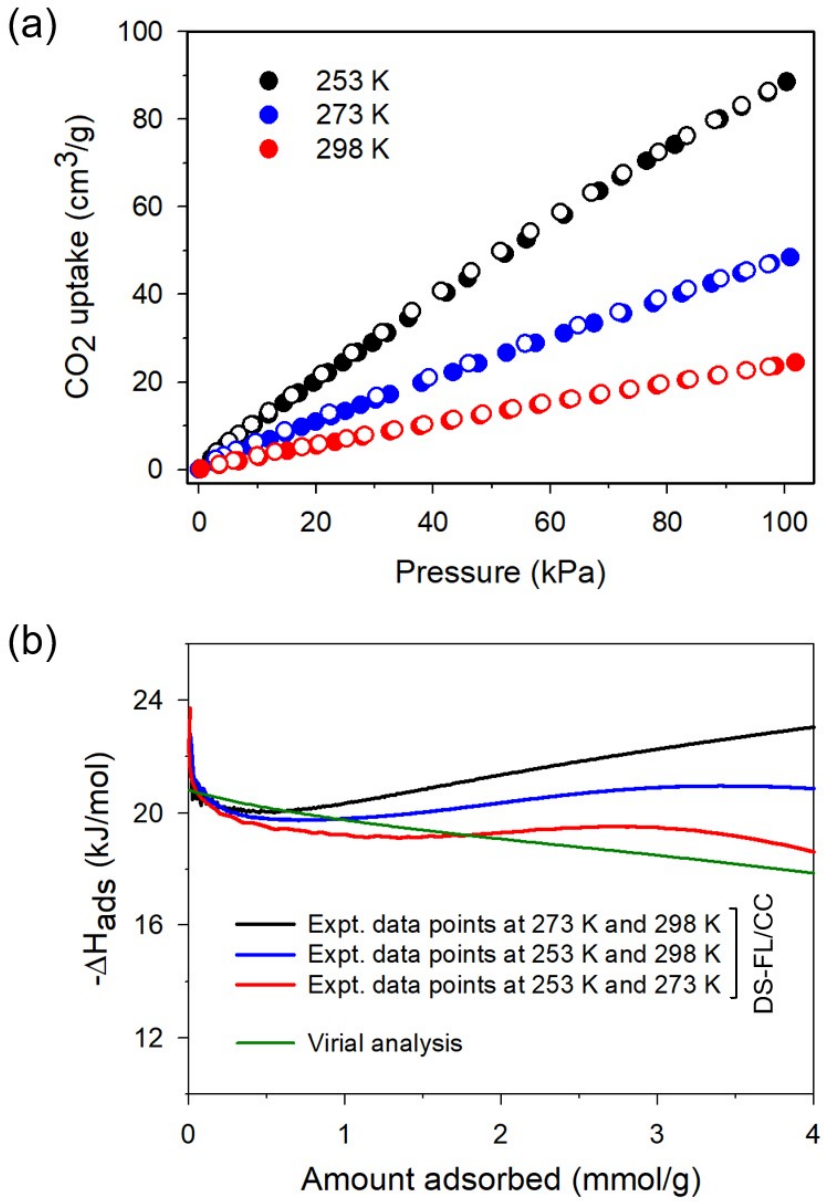

Fig. S29. CO_2 adsorption on Cu-ZIF-**rho**. (a) Measured CO_2 gas adsorption-desorption isotherms at three different temperatures, where the absorption branches are marked with filled circles. (b) Isosteric enthalpy plots of CO_2 adsorption from a DS-FL/CC method and the Virial analysis, respectively.[S18]

Table S12. The high-pressure gas adsorption capacity of Cu-ZIF-**rho**. The X-ray density (0.971 g/cm^3) was used for the conversion between the gravimetric and volumetric capacities.

Gas	Gas adsorption capacity at T = 273 K						
	Excess			Total			P
	(cm^3/g)	(cm^3/cm^3)	(mmol/g)	(cm^3/g)	(cm^3/cm^3)	(mmol/g)	(bar)
H_2	29.7	28.8	1.326	76.9	74.7	3.433	83
CH_4	112	109	5.000	173	168	7.723	83
CO_2	238	231	10.625	264	256	11.786	32
Gas	**Gas adsorption capacity at T = 298 K**						
	Excess			Total			P
	(cm^3/g)	(cm^3/cm^3)	(mmol/g)	(cm^3/g)	(cm^3/cm^3)	(mmol/g)	(bar)
H_2	24.7	24.0	1.103	69.2	67.2	3.089	85
CH_4	99	96	4.420	151	147	6.741	85
CO_2	182	177	8.125	224	218	10.000	51

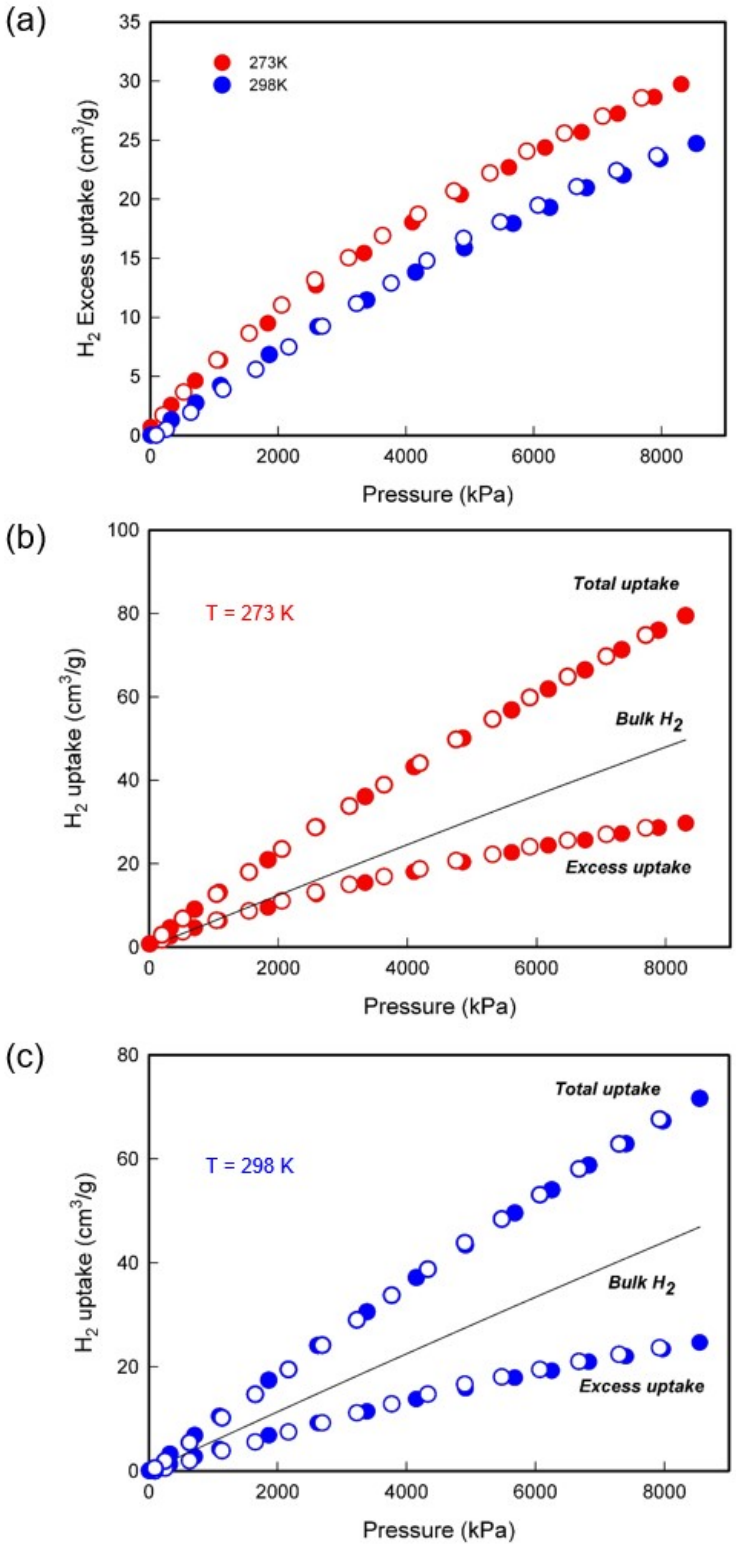

Fig. S30. (a) H_2 gas excess adsorption-desorption isotherms up to ~80 bar for Cu-ZIF-**rho**. The absorption branches are marked with filled circles. Total and excess H_2 gas adsorption-desorption data at (b) 273 K and (c) 298 K, respectively.

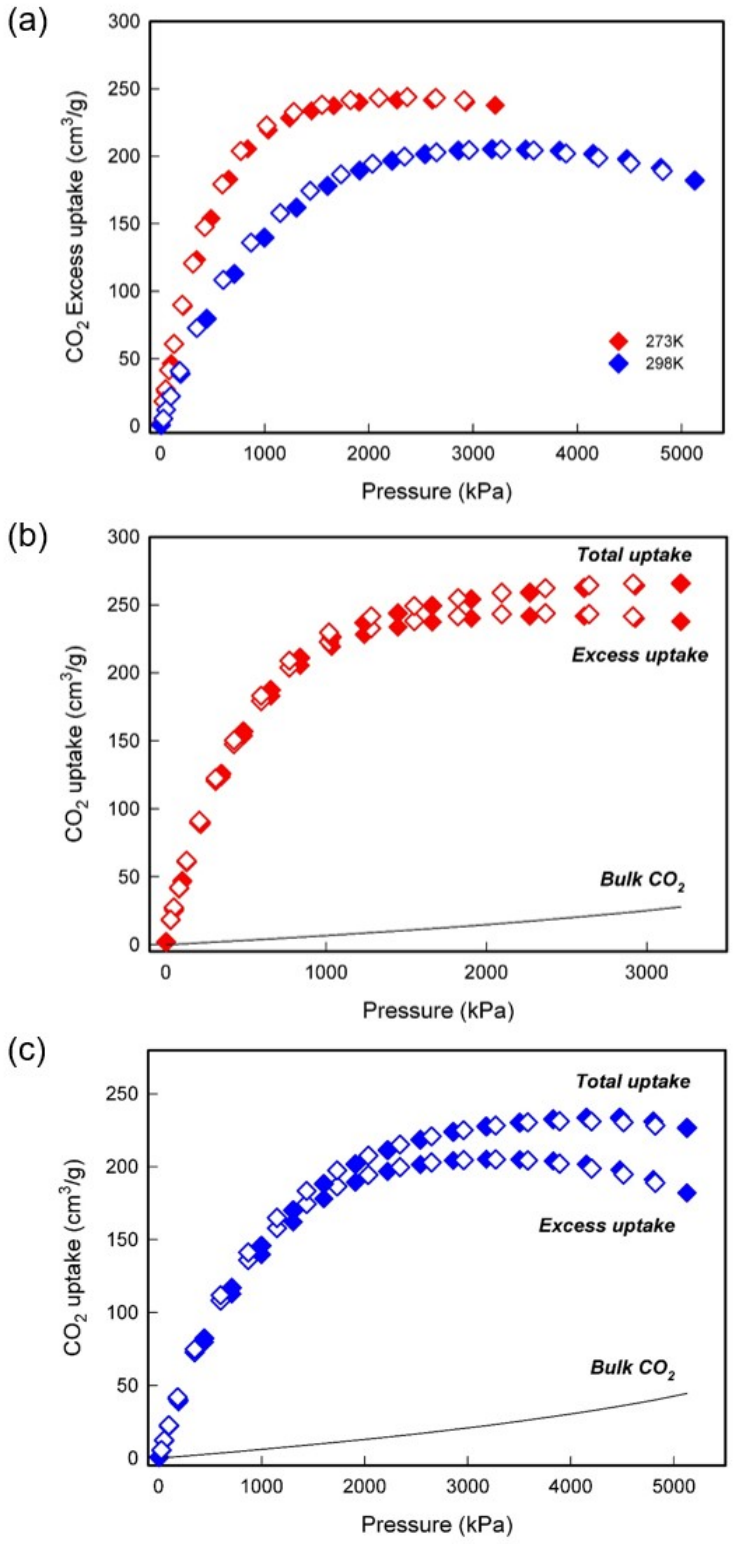

Fig. S31. (a) CO_2 gas excess adsorption-desorption isotherm measured at high pressure for Cu-ZIF-**rho**. The absorption branches are displayed with filled marks. Total and excess CO_2 gas adsorption-desorption data at (b) 273 K and (c) 298 K, respectively.

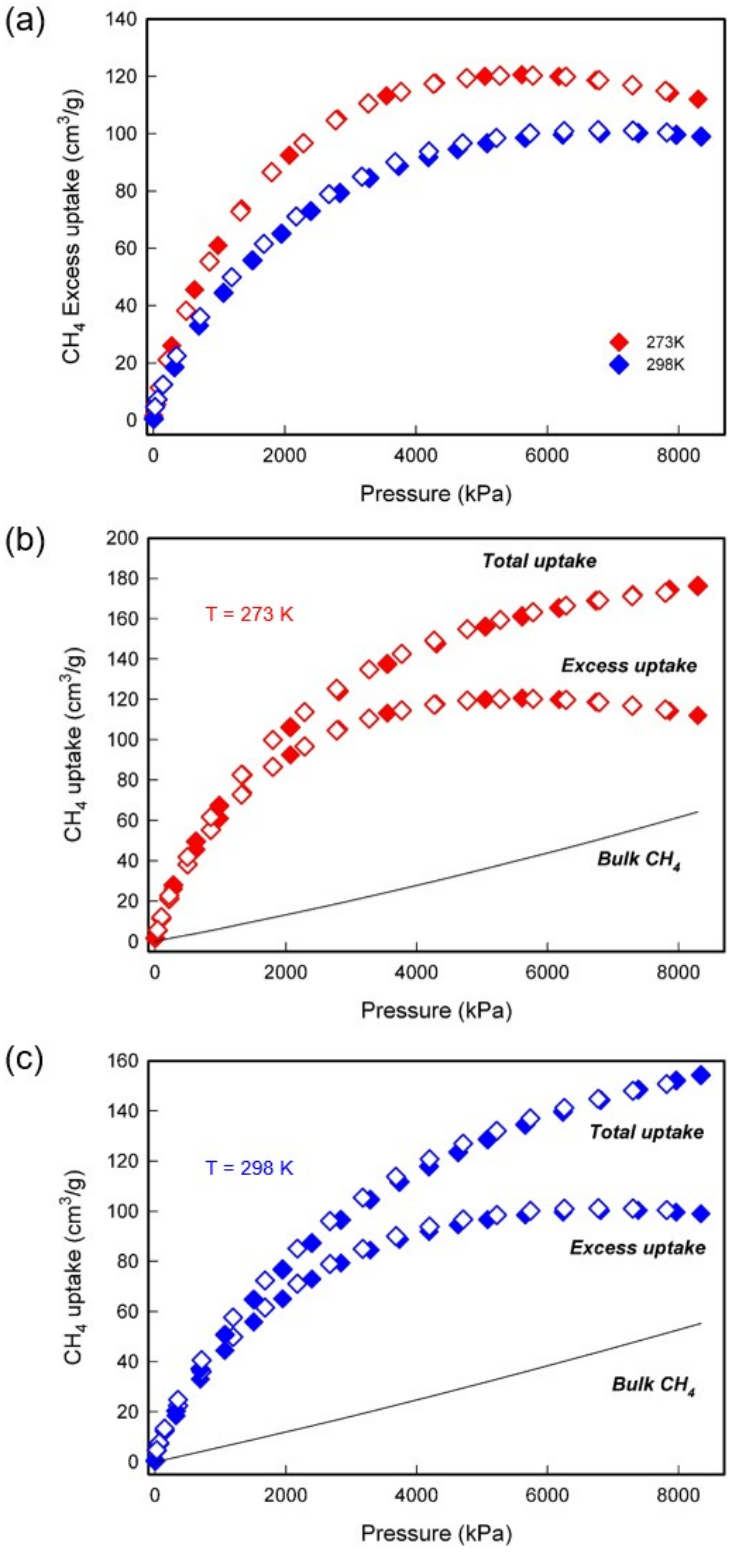

Fig. S32. (a) CH_4 gas excess adsorption-desorption isotherms up to ~80 bar for Cu-ZIF-**rho**. The absorption branches are marked with filled circles. Total and excess CH_4 gas adsorption-desorption data at (b) 273 K and (c) 298 K, respectively.

References

S1. Arvai, A. J.; Nielsen, C. ADSC Quantum-210 ADX Program, Area Detector System Corporation; Poway, CA, USA, **1983**.

S2. Otwinowski, Z.; Minor, W.; in Methods in Enzymology, ed. Carter, Jr., C. W.; Sweet, R. M. Academic Press, New York, 1997, vol. 276, part A, pp. 307.

S3. Sheldrick, G. M. A short history of SHELX. *Acta Cryst.* **2008**, *A64*, 112.

S4. Spek, A. L. *Acta Cryst.* **2009**, *D65*, 148.

S5. Sheldrick, G. M. Acta Cryst. **2015**, *C71*, 3.

S6] Masciocchi, N.; Bruni, S.; Cariati, E.; Cariati, F.; Galli, S.; Sironi, A. *Inorg. Chem*. **2001**, *40*, 5897−5905.

S7. Tian, Y.-Q.; Yao, S.-Y.; Gu, D.; Cui, K.-H.; Guo, D.-W.; Zhang, G.; Chen, Z.-X.; Zhao, D.-Y. *Chem. Eur. J*. **2010**, *16*, 1137–1141.

S8. Biswal, B. P.; Panda, T.; Banerjee, R. *Chem. Commun*. **2012**, *48*, 11868–11870.

S9. Banerjee, R.; Phan, A.; Wang, B.; Knobler, C.; Furukawa, H.; O'Keeffe, M.; Yaghi, O. M. *Science* **2008**, *319*, 939−943.

S10. Yang, J.; Zhang, Y.; Liu, Q.; Trickett, C. A.; Gutierrez-Puebla, E.; Monge, M. Á.; Cong, H.; Aldossary, A.; Deng, H.; Yaghi, O. M. *J. Am. Chem. Soc*. **2017**, *139*, 6448−6455.

S11. Nguyen, N. T. T.; Furukawa, H.; Gándara, F.; Nguyen, H. T.; Cordova, K. E.; Yaghi, O. M. *Angew. Chem. Int. Ed*. **2014**, *53*, 10645−10648.

S12. Park, K. S.; Ni, Z.; Côté, A. P.; Choi, J. Y.; Huang, R.; Uribe-Romo, F. J.; Chae, H. K.; O'Keeffe, M.; Yaghi, O. M. *Proc. Natl. Acad. Sci. U.S.A*. **2006**, *103*, 10186–10191.

S13. Hayashi, H.; Côté, A. P.; Furukawa, H.; O'Keeffe, M.; Yaghi, O. M. *Nat. Mater*. **2007**, *6*, 501–506.

S14. Oh, H.; Savchenko, I.; Mavrandonakis, A.; Heine, T.; Hirscher, M. *ACS Nano* **2014**, *8*, 761–770.

S15. Falconer, J. L.; Madix, R. J. *Surf. Sci*. **1975**, *48*, 393–405.

S16. BIOVIA, Dassault Systèmes, Materials Studio, 22.1.0.3462, San Diego: Dassault Systèmes, 2022.

S17. Düren, T.; Millange, F.; Férey, G.; Walton, K. S.; Snurr, R. Q. *J. Phys. Chem. C* **2007**, *111*, 15350–15356.

S18. Nuhnen, A.; Janiak, C. *Dalton Trans*. **2020**, *49*, 10295–10307.